Cluster observations of band-limited Pc 1 waves associated with streaming H + and O + ions in the high-altitude plasma mantle

M J Engebretson, C.R.G. Kahlstorf, D.L. Murr, J L Posch, A. Keiling, B. Lavraud, H. Rème, M. R. Lessard, E.-H. Kim, J.R. Johnson, et al.

Cluster observations of band-limited Pc 1 waves associated with streaming H^+ and O^+ ions in the high-altitude plasma mantle

M. J. Engebretson,[1] C. R. G. Kahlstorf,[1,2] D. L. Murr,[1] J. L. Posch,[1] A. Keiling,[3] B. Lavraud,[4] H. Rème,[4] M. R. Lessard,[5] E.-H. Kim,[6] J. R. Johnson,[6] J. Dombeck,[7] B. Grison,[8] P. Robert,[9] K.-H. Glassmeier,[10] and P. M. E. Décréau[11]

Received 31 May 2012; revised 24 August 2012; accepted 27 August 2012; published 12 October 2012.

[1] Bursts of band-limited Pc 1 waves (0.2 to ~1.0 Hz) with normalized frequency $f/f_{H+} \sim 0.5$ have been observed by the Cluster spacecraft during many passes through the high-latitude plasma mantle. These transverse, left-hand polarized waves are associated with regions of H^+ and O^+ ions streaming away from Earth along magnetic field lines at the same velocity (~140 km/s). Waves were observed only when H^+ fluxes increased by factors of 10–1000 and energies of both ion species increased by factors of up to 10. We present two satellite-ground conjunctions to demonstrate the high latitude localization of these waves and their ability to reach the polar ionosphere and two extended examples of waves and associated ion distribution functions near the southern dusk flank magnetopause. We also present the results of a search for all such events during Cluster's 2002 and 2003 passages through the magnetotail, with orbital precession covering dawn to dusk on Earth's night side (June through December). A total of 46 events (band-limited Pc 1–2 waves accompanied by a sustained population of streaming H^+ and O^+ ions, separated by at least 12 min) were observed on 29 days. The waves were generally associated with intervals of southward IMF Bz and/or large IMF By (times of active cusp reconnection), and often but not always occurred during the main phase or early recovery phase of magnetic storms. Analysis of selected events shows that the waves are associated with large H^+ temperature anisotropy, and that the waves propagate opposite to the direction of the streaming ions. A wave instability analysis using the WHAMP code confirms that the generation of these waves, via the ion cyclotron instability, is basically consistent with known physics. Their extended region of wave growth is likely, however, to reach tailward significantly beyond the Cluster orbit.

Citation: Engebretson, M. J., et al. (2012), Cluster observations of band-limited Pc 1 waves associated with streaming H+ and O+ ions in the high-altitude plasma mantle, *J. Geophys. Res.*, *117*, A10219, doi:10.1029/2012JA017982.

1. Introduction

[2] Although most Pc 1–2 waves (0.1–5.0 Hz) observed in Earth's magnetosphere occur on closed field lines and are driven by ring current or plasma sheet ions that convect sunward from the magnetotail [cf. the reviews of *Kangas et al.*, 1998; *Fraser et al.*, 2006], such waves have also been observed in the plasma mantle, poleward of the cusp region [*Menk et al.*, 1992; *Dyrud et al.*, 1997; *Engebretson et al.*, 2009], in association with upgoing, reflected cusp ions using data from the Polar satellite [*Engebretson et al.*, 2005]. In this paper we present observations of similar waves at higher altitudes in the mantle/lobe regions using data from the Cluster spacecraft. These waves are collocated with H^+ and O^+ ions

[1]Department of Physics, Augsburg College, Minneapolis, Minnesota, USA.
[2]Now at AT&T Inc., Bloomington, Minnesota, USA.
[3]Space Sciences Laboratory, University of California, Berkeley, California, USA.
[4]Institut de Recherche en Astrophysique et Planétologie, Université de Toulouse, CNRS, Toulouse, France.

Corresponding author: M. J. Engebretson, Department of Physics, Augsburg College, 2211 Riverside Ave., Minneapolis, MN 55454, USA. (engebret@augsburg.edu)

0148-0227/12/2012JA017982

[5]Space Science Center and Department of Physics, University of New Hampshire, Durham, New Hampshire, USA.
[6]Princeton Plasma Physics Laboratory, Princeton University, Princeton, New Jersey, USA.
[7]Department of Physics, University of Minnesota, Minneapolis, Minnesota, USA.
[8]Institute of Atmospheric Physics, Academy of Sciences of the Czech Republic, Prague, Czech Republic.
[9]Laboratoire de Physique des Plasmas, CNRS, Ecole Polytechnique, UPMC, P11, Vélizy, France.
[10]Institute for Geophysics and Extraterrestrial Physics, Technische Universität Braunschweig, Braunschweig, Germany.
[11]Laboratoire de Physique et Chimie de l'Environnement et de l'Espace, CNRS, UMR 6115, Orléans, France.

streaming away from Earth along magnetic field lines at nearly the same velocity (~140 km/s). These particle signatures have been identified in a number of earlier studies of the ion populations in the plasma mantle, but they have never before been associated with Pc 1–2 waves.

[3] The plasma mantle, a persistent layer of tailward-flowing magnetosheath-like plasma inside of and adjacent to the magnetopause, extending over the entire surface of the magnetosphere tailward of the polar cusp, was first identified by *Rosenbauer et al.* [1975] using data from the Heos 2 spacecraft. This study noted that flow speeds of protons in the mantle were roughly half those of the adjacent magnetosheath, and mantle protons were normally significantly cooler along B than perpendicular to it, i.e., $T_{\|} < T_{\perp}$. Farther down the magnetotail, *Hardy et al.* [1975], using data from ion detectors deployed on the lunar surface during the Apollo missions, found an extensive region of low energy antisunward plasma flow in the tail lobe adjacent to the magnetopause.

[4] *Rosenbauer et al.* [1975] suggested that the combination of two phenomena, penetration of magnetosheath plasma into the cusp and simultaneous and subsequent tailward convection, provided the most natural explanation for the existence of the plasma mantle as well as for its gross features. More recent works, however, have demonstrated the role of reconnection in driving both plasma entry and subsequent convection direction and magnitude in the cusp/mantle region (which can be sunward for northward IMF), as synthesized in the statistical works of *Lavraud et al.* [2004, 2005]. Observations by the Cluster spacecraft also made clear that because the formation of the plasma mantle relies on tailward convection, it is absent under conditions of northward IMF and dominantly sunward convection [*Lavraud et al.*, 2002; *Cargill et al.*, 2005]. The importance of the plasma mantle and this population of streaming ions of solar wind origin for magnetospheric dynamics was first underscored by *Pilipp and Morfill* [1978], who calculated, using two different models, that the observed ion fluxes in the plasma mantle were more than adequate to supply plasma to the plasma sheet in Earth's magnetotail. *Borovsky et al.* [1998] provide several lines of evidence supporting this connection between the solar wind and the plasma sheet.

[5] Ion spectrometer observations using ISEE 2 data reported by *Candidi et al.* [1982] revealed that H^+, He^+, and O^+ ions in the northern dawnside magnetotail lobe ($-15\ R_E > X > -23\ R_E$) were streaming with nearly equal velocities. Over a decade later *Seki et al.* [1996], using Geotail satellite data, reported H^+, He^+, He^{++}, and O^+ streaming tailward with roughly the same flow velocity deep in the magnetotail (~159 R_E), and *Hirahara et al.* [1996], based on similar Geotail observations in the magnetotail lobe region, from $X_{GSM} \sim -10$ to $-210\ R_E$, inferred that the cold ion beams of ionospheric origin merged with the solar wind component penetrating to the magnetosphere at the mantle or the flank of the tail lobe.

[6] The near equality of velocities can be attributed to the action of a "geomagnetic mass spectrometer" [*Horwitz and Lockwood*, 1985; *Horwitz*, 1986]. Ions disperse according to their velocity because of an $\mathbf{E} \times \mathbf{B}$ filter: only a particular energy ion reaches a particular tail lobe location.

[7] *Orsini et al.* [1987] summarized ISEE observations that both ions of ionospheric origin (mainly O^+ and H^+) and solar wind origin (mainly H^+ and He^{++}) flow with roughly the same velocities in the mantle, and inferred that both populations entered the mantle near the polar cusp. *Seki et al.* [2000] reached similar conclusions: they noted that the proton density was enhanced during southward IMF, presumably because the plasma enters preferentially through open field lines which have been recently reconnected at the dayside magnetopause. However, they pointed out that the observed energy of O^+ was considerably higher than the typical energy of cusp/cleft outflows, suggesting that further energization mechanisms might be involved [*Seki et al.*, 1998]. *Orsini et al.* [1987] also noted that the observed flow velocities were at the high-energy end of the distribution of ions accelerated upward from the ionosphere, and at the low-energy end of the distribution of solar wind ions outside the magnetosphere.

[8] *Cladis* [1986] showed that the velocity component of ions escaping from the cusp ionosphere can be increased by more than an order of magnitude by field-aligned acceleration due to the component of the convection velocity ($\mathbf{V}_E = \mathbf{E} \times \mathbf{B}/B^2$) in the direction of $d\boldsymbol{e}/dt$, where $\boldsymbol{e}$ is the unit vector in the direction of the local magnetic field, because of the curvature of this field in the high-altitude mantle/lobe region. This acceleration mechanism is independent of the mass or charge of the ion. *Cladis et al.* [2000], in a follow up study, used data from the Polar satellite along with a computer simulation to confirm this mass- and charge-independent acceleration mechanism. Finally, we note that *Candidi et al.* [1988] reported on the basis of ISEE-2 observations that O^+ streams were more frequently observed on the dusk side of the magnetosphere. A recent comprehensive study of the occurrence and location of O^+ streams by *Liao et al.* [2010] based on Cluster satellite observations found a similar preference for dusk-side occurrence, especially during storm recovery phase.

[9] In section 3 of this paper we present two examples of Pc 1 waves poleward of the cusp and of associated ion distributions observed by the Cluster spacecraft, simultaneous with ground-based magnetometer observations. In section 4 we present Cluster observations of magnetic field and ion distribution parameters for two more extended intervals of such waves associated with streaming H^+ and O^+ ions, at higher altitudes, and provide evidence that these waves may be driven by the ion cyclotron instability. In section 5 we show the results of a systematic search for these wave events in the first 2 years of Cluster's tail passage. We find that the 46 Pc 1–2 events identified on 29 days are consistent in their association with streaming H^+ and O^+ ions, and all occur near the magnetopause boundary tailward of the cusp, in locations consistent with dayside reconnection as a source for the streaming protons. In section 6 we present an instability analysis and conclude with a discussion of the probable propagation mode of these waves.

2. Data Set

[10] The four spacecraft of the Cluster mission were launched in late summer 2000 into highly elliptical polar orbits with apogee of 19.6 R_E, perigee of 4 R_E, and 57-h period [*Escoubet et al.*, 2001]. The interspacecraft separation varied from 100 to 10,000 km throughout the mission. The FGM instrument on each Cluster spacecraft [*Balogh et al.*, 2001] consists of redundant triaxial fluxgate magnetic field sensors on one of two radial booms; it measures the vector magnetic field magnitude and direction with a resolution up to 67 samples per second, and at 22.416 samples per second

Table 1. Locations of the Ground-Based Magnetometers Used in This Study, Updated to Epoch 2004 at 100 km Altitude

Site	Geographic		Geomagnetic		UT of Local Magnetic Noon
	Lat.	Long.	Lat.	Long.	
South Pole	90 S	—	74.2 S	18.5 E	1536
McMurdo	77.9 S	166.7 E	80.0 S	326.9 E	1900
AGO P1	83.9 S	129.6 E	80.2 S	16.8 E	1546

in nominal mode. The Cluster Ion Spectroscopy (CIS) experiment [*Rème et al.*, 2001] is composed of a time-of-flight Composition and Distribution Ion Function analyzer, CODIF, which can determine the energy, composition, and three-dimensional distributions of the major magnetospheric ions (H^+, He^+, He^{++} and O^+) in the energy range from 0 to 40 keV, and a Hot Ion Analyzer (HIA), which does not resolve mass but has higher energy and angular resolution. The Electric Field Waveform (EFW) instrument is composed of two pairs of probes on wire booms. It measures two components of the electric field in the spacecraft spin plane at a normal sampling rate of 25 (or 450 in high bit rate) vectors per second [*Gustafsson et al.*, 2001]. The waves of high frequency and sounder for probing of electron density by relaxation (WHISPER) instrument [*Décréau et al.*, 1997] provides a combination of active sounding and passive surveys of natural plasma emissions that can provide a time resolution for the determination of total electron density of 2.2 s in normal telemetry mode and 0.3 s in burst mode, respectively.

[11] The wave events to be shown in sections 3 and 4 were identified during a visual scan of operational survey plots of FGM data. A later survey of all the high time resolution Cluster FGM data during the first 2 years of Cluster's passage through the magnetotail, with orbital precession covering dawn to dusk on Earth's night side (June through December of 2002 and June through November of 2003), led to the identification of two categories of band-limited wave activity in the Pc 1–2 frequency band in the magnetotail and polar

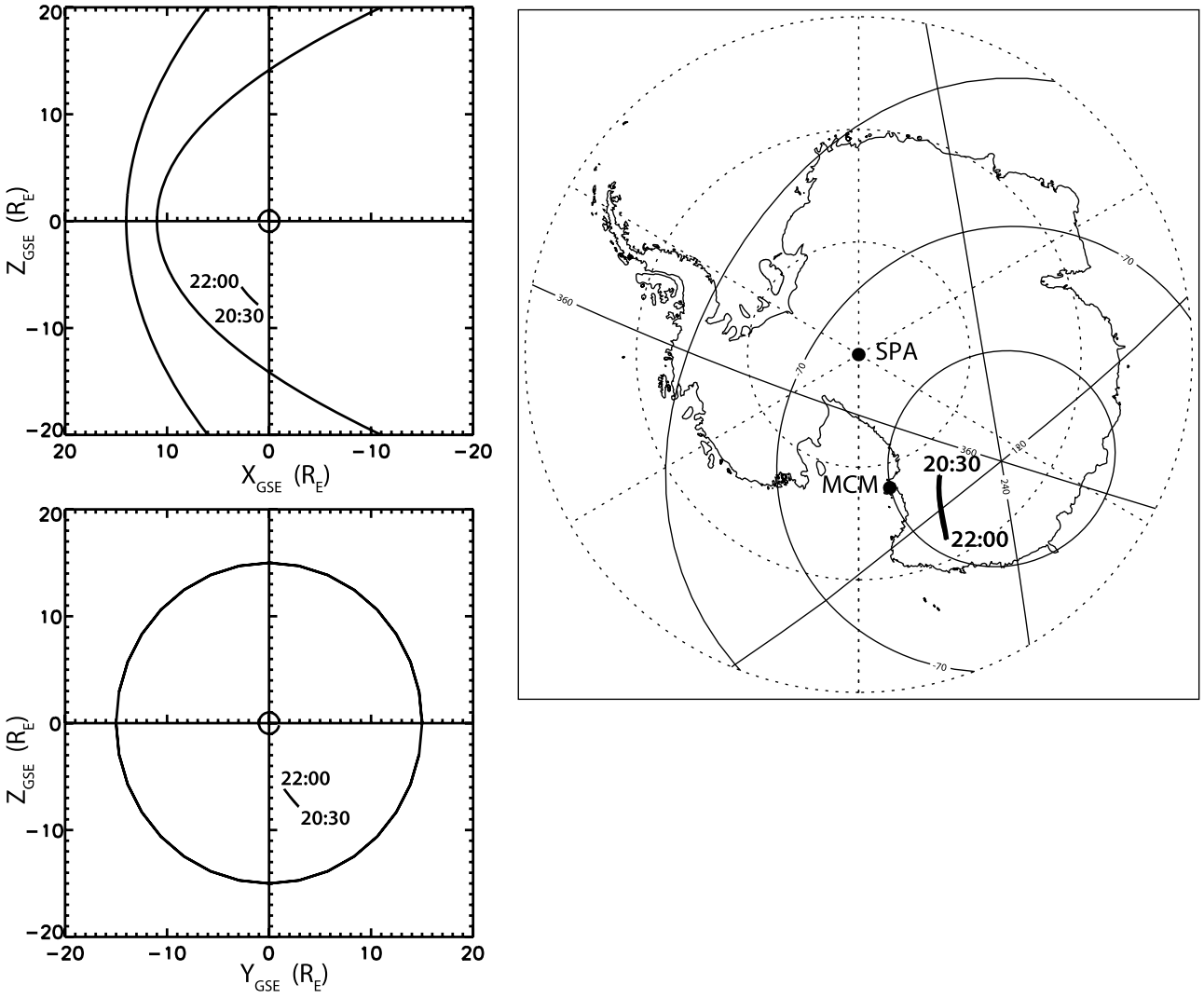

Figure 1. Orbit of the Cluster 1 spacecraft from 2030 to 2200 UT 30 September 2003 (YRDAY 03273). (top left) The projection in the GSE X–Z plane, and (bottom left) the projection in the GSE Y–Z plane. (right) The projection of the magnetic field lines traversed by Cluster 1 during this interval, onto the Antarctic ionosphere. The locations of McMurdo and South Pole Station are also indicated.

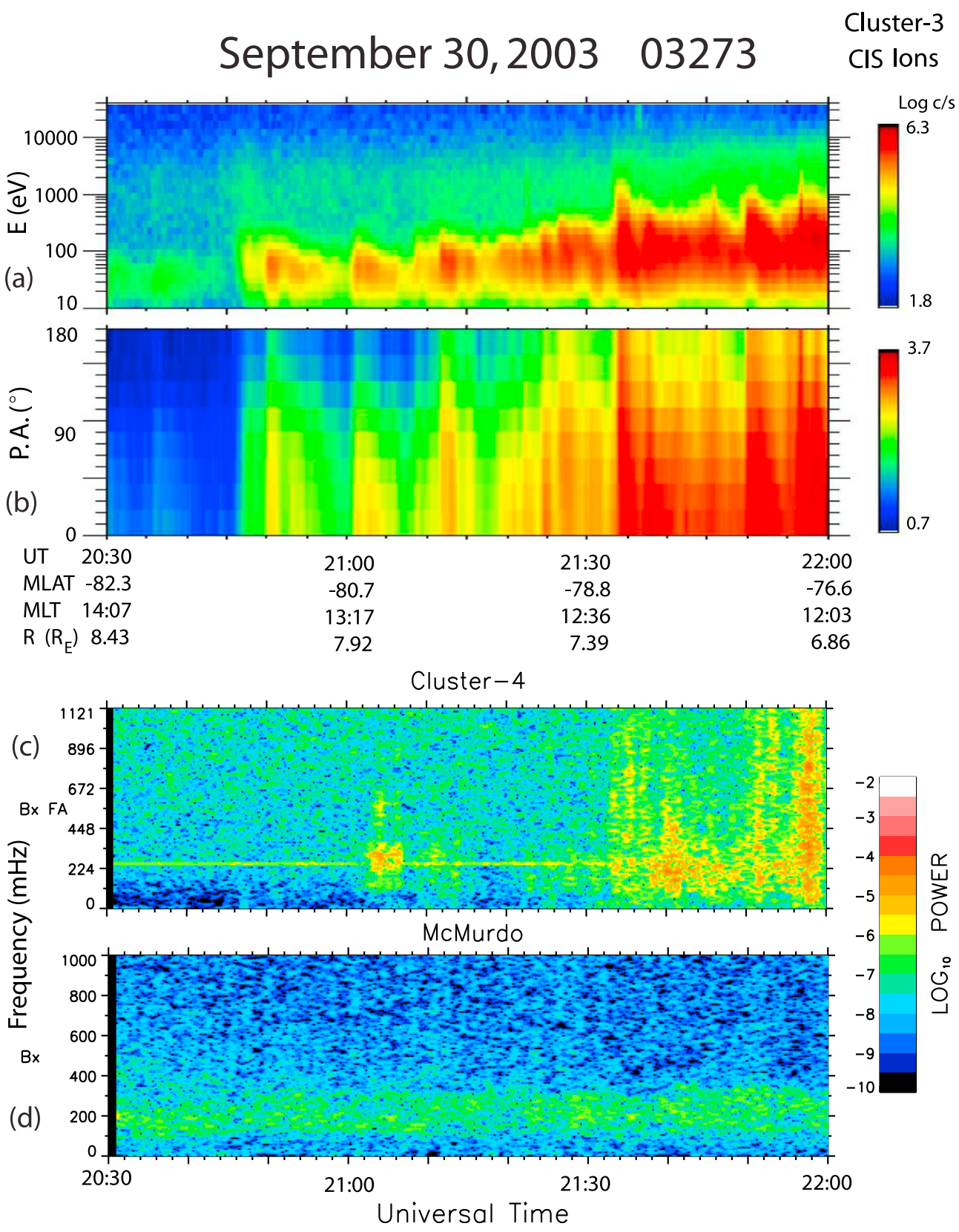

Figure 2. (a) Energy spectrogram of omnidirectional fluxes and (b) pitch angle spectrogram of ions observed by the CIS instrument on Cluster-3. Fourier spectrogram of (c) the X component of FGM magnetic field data (in mean field-aligned coordinates) from Cluster-4 and (d) the X (north-south) component from McMurdo, Antarctica, from 2030 to 2200 UT 30 September 2003.

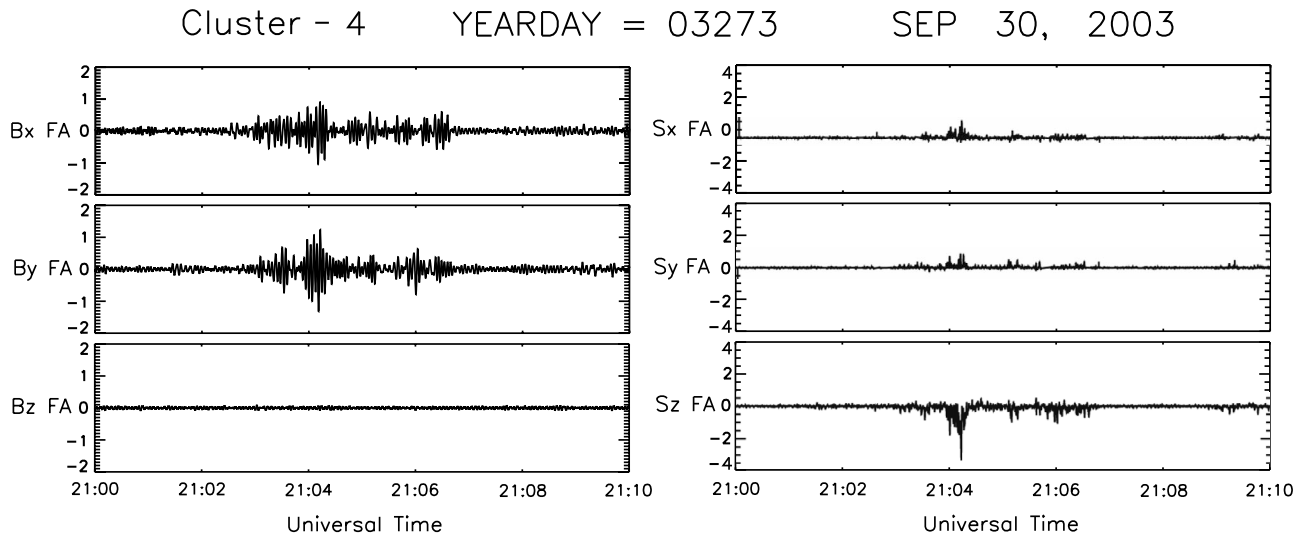

Figure 3. (a) Bandpass-filtered (0.1–0.4 Hz) plot of magnetic field data in nanoTeslas obtained by Cluster 4, in field-aligned coordinates, from 2100 to 2110 UT 30 September 2003. (b) Poynting vectors in field-aligned coordinates, in Watts/km^2, for this same time interval.

cap/tail lobe regions, respectively. Examples of the first of these categories, multiple-harmonic waves with fundamental at the local proton gyrofrequency observed in the plasma sheet boundary layer, were presented by *Broughton et al.* [2008] and *Engebretson et al.* [2010]; the latter paper also presented a statistical study of these events. A theoretical analysis of the instabilities responsible for their generation was presented in a companion paper by *Denton et al.* [2010].

[12] Ground-based observations of mantle waves presented here were obtained from three search coil magnetometers in Antarctica operated by Augsburg College and the University of New Hampshire: South Pole Station, McMurdo, and AGO P1, an automatic geophysical observatory deployed as part of the Polar Experiment Network for Geophysical Upper Atmosphere Interactions (PENGUIn) [*Engebretson et al.*, 1997, 2005]. Data from these stations (Table 1) were obtained in local geomagnetic coordinates; only X component data (aligned north-south) will be presented here.

3. Cluster—Ground Conjunctions

[13] In this section we present two examples of Pc 1–2 wave signals observed simultaneously by the Cluster spacecraft and by ground-based search coil magnetometers in Antarctica when the magnetic footpoint of Cluster passed near to the ground stations.

3.1. Event 1: 30 September 2003

[14] Near the end of 30 September 2003, the Cluster spacecraft passed sunward from the dusk sector southern polar cap, across the midaltitude cusp/cleft region, and into the southern dayside magnetosphere near local noon, as shown in Figure 1. During the highlighted interval shown in Figure 1 (2030–2200 UT), the Cluster spacecraft passed sunward from the southern polar cap, through the plasma mantle, and into the cusp. The Antarctic footpoint of the Cluster trajectories passed ~15° westward of McMurdo, Antarctica, which was in the nominal polar cap at ~1400 magnetic local time during this interval. The GSM y component of the interplanetary magnetic field (IMF By) was near 5.0 nT during the entire interval, and IMF Bz was within 2 nT of 0.

[15] Figure 2 shows Cluster particle and ULF wave data from 2030 to 2200 UT, as well as wave data from the Augsburg College/University of New Hampshire search coil magnetometer at McMurdo. Figures 2a and 2b show energy and pitch angle spectrograms of Cluster-3 HIA ion data. The pitch angle is the angle between the ion velocity vector and the magnetic field vector. In the southern polar regions, as in this case, pitch angles near 0° correspond to particles with velocity components parallel to the magnetic field, hence with upward motion. During the time interval shown, Cluster-3 moved from the polar cap toward lower magnetic latitudes shortly after local noon MLT, and encountered ion bursts with center energy gradually increasing from ~60 eV to ≥1 keV. These ion bursts were predominantly upgoing at first, but included more downgoing fluxes as the satellite moved toward lower latitudes near 2200 UT. These ion distributions are typical of the midaltitude plasma mantle and cusp, respectively [e.g., *Rosenbauer et al.*, 1975; *Engebretson et al.*, 2005].

[16] Figures 2c and 2d show frequency-time Fourier spectrograms of differenced ULF wave power from Cluster-4 and McMurdo, Antarctica, color coded according to the color bar at the right, in the range from 0 to 1.1 Hz and 0 to 1.0 Hz, respectively. Cluster data are presented in local mean field-aligned coordinates (averaged over 7500 points, or roughly 5.5 min). The X and Y components are transverse to the field-aligned coordinate, Z, with X radially outward and Y azimuthal. Waves near 0.25 Hz appeared at McMurdo throughout the 1.5-h interval with modestly varying amplitude, and appeared at Cluster in association with bursts of upgoing ~50-eV ions poleward of the cusp near 2104 and 2140–2145 UT.

[17] Details of the waves observed near 2104 UT are shown in Figure 3. Figure 3a is a plot of band-pass filtered (0.1–0.4 Hz) magnetic field data in field-aligned coordinates

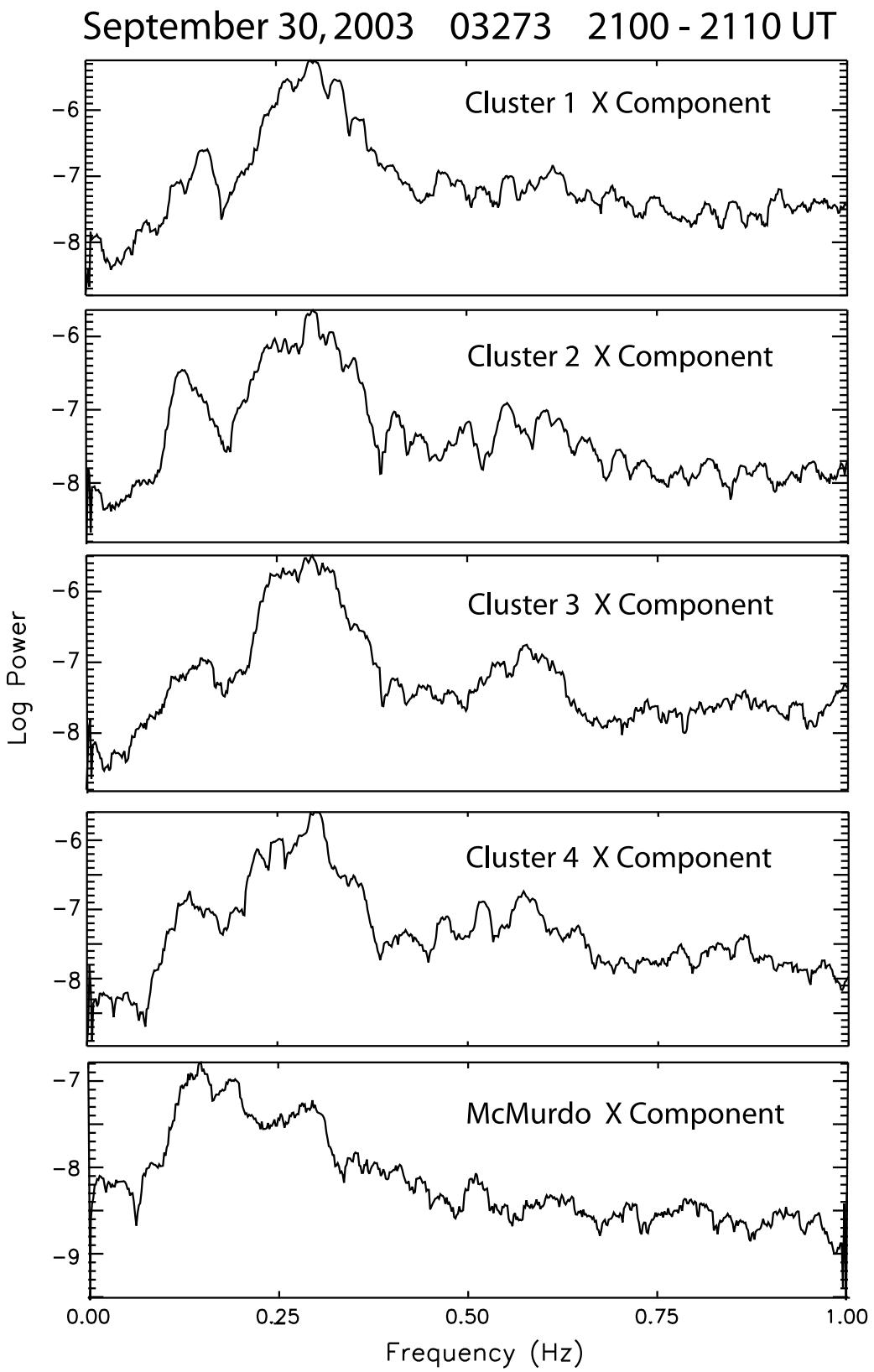

Figure 4. Stacked plots of Fourier spectra of the X component of differenced magnetic field data in field-aligned components from Cluster-1. -2, -3, -4 (top four panels, respectively), and of the north-south component of search coil data from McMurdo, Antarctica, for the interval 2100 to 2110 UT 30 September 2003.

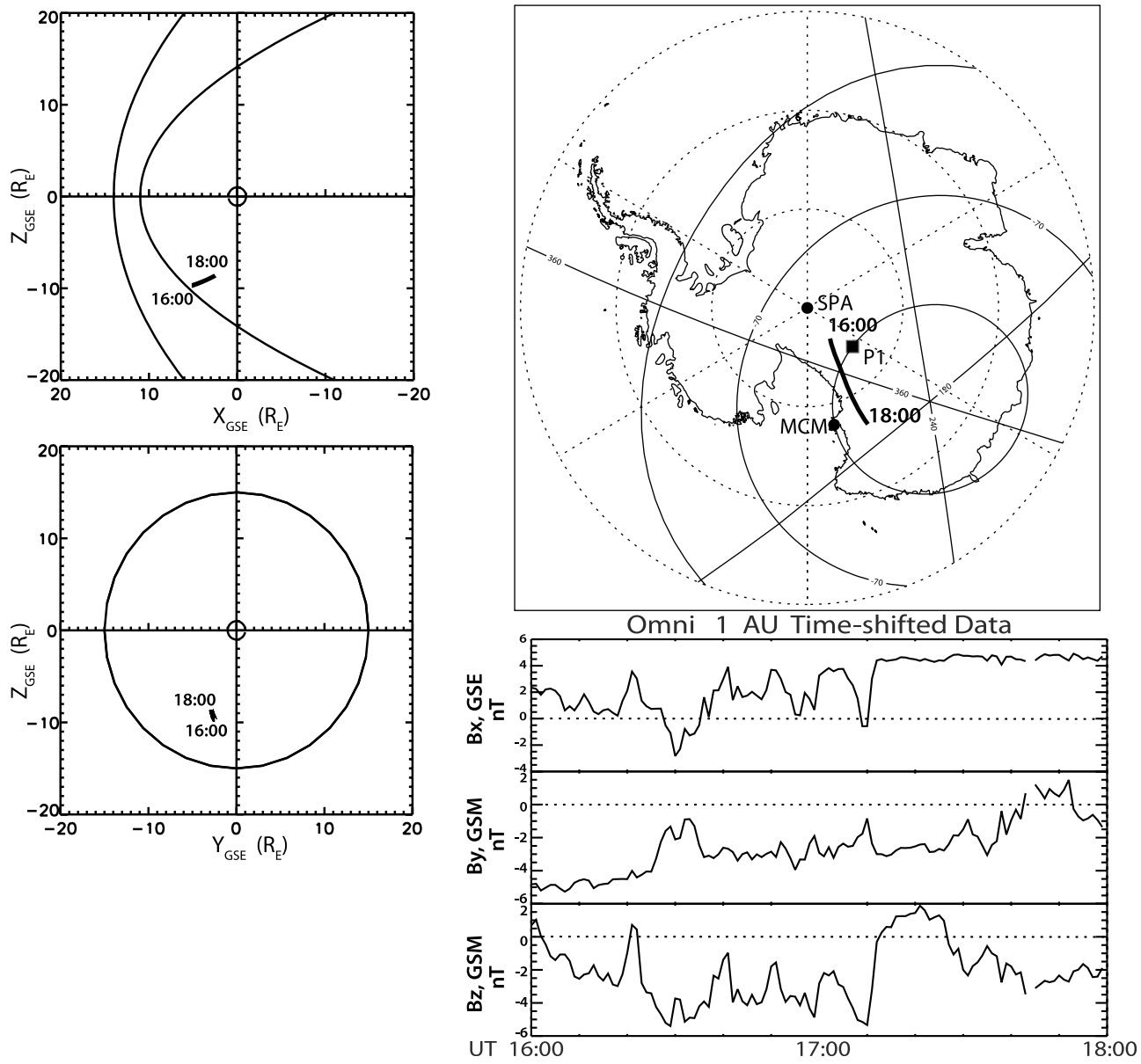

Figure 5. Orbit of the Cluster 1 spacecraft from 1600 to 1800 UT 15 February 2004 (YRDAY 04046). (top left) The projection in the GSE X–Z plane, and (bottom left) the projection in the GSE Y–Z plane. (top right) The projection of the magnetic field lines traversed by Cluster 1 during this interval, onto the Antarctic ionosphere. The locations of McMurdo, South Pole Station, and AGO P1 are indicated. (lower right) IMF data time-shifted to the nose of Earth's magnetosphere (from the OMNI data base).

from Cluster 4, from 2100 to 2110 UT 30 September 2003, which indicates that the wave was purely transverse. Figure 3b shows the components of the Poynting vector, also in field-aligned coordinates. Principal power was in the Z (field-aligned) component (bottom panel) and in the negative direction, hence antiparallel to **B** and downward/Earthward.

[18] Figure 4 shows stacked Fourier spectra of the X component of differenced magnetic field data in field-aligned components from Cluster-1, -2, -3, and -4, respectively, and of the north-south component of search coil data from McMurdo, Antarctica, for the interval 2100 to 2110 UT on this day. Wave power was enhanced from ~0.1 to 0.35 Hz at all four closely spaced Cluster spacecraft and at McMurdo, with recognizable peaks near 0.15 and 0.30 Hz, but the largest power was near 0.30 Hz at Cluster and near 0.15 Hz at McMurdo. South Pole Station, located at near-cusp magnetic latitude but at this time quite distant from local noon (~1800 MLT), observed no Pc 1–2 wave activity.

3.2. Event 2: 15 February 2004

[19] On this day the Cluster spacecraft passed tailward through the prenoon cusp/cleft region from their apogee in the upstream solar wind, and into the southern mantle and polar cap on their way to perigee near midnight. Figure 5 shows the path of Cluster on this day, and highlights the interval from 1600 to 1800 UT. Its modeled ground track moved from poleward of South Pole Station (CGMLAT 74.3°) and AGO P1 (CGMLAT 80.4°), toward McMurdo

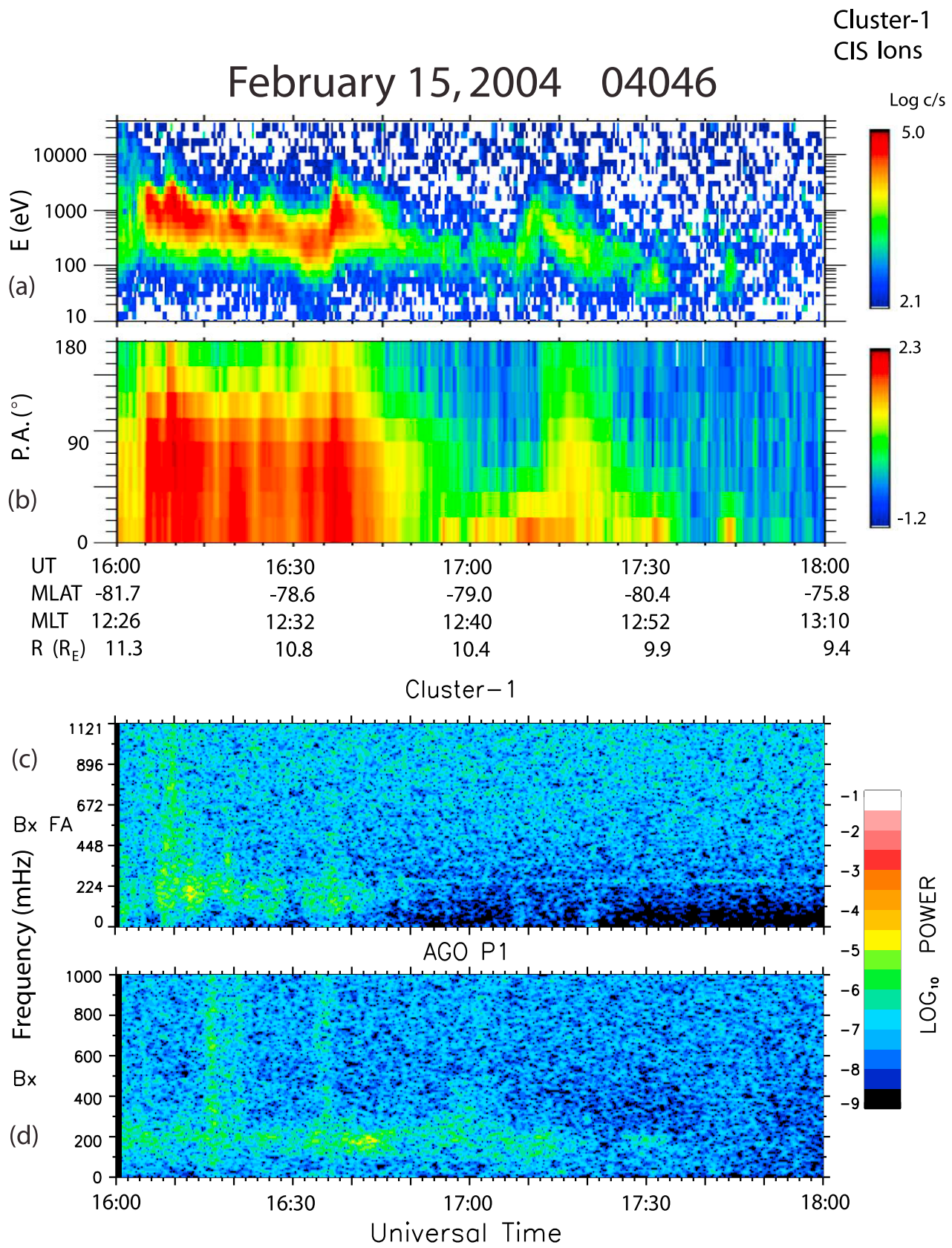

Figure 6. (a) Energy spectrogram of omnidirectional fluxes and (b) pitch angle spectrogram of ions observed by the CIS instrument on Cluster-1. Fourier spectrogram of (c) the X component of FGM magnetic field data in mean field-aligned coordinates from Cluster-1 and (d) the X (north-south) component from AGO P1, Antarctica, from 1600 to 1800 UT 15 February 2004.

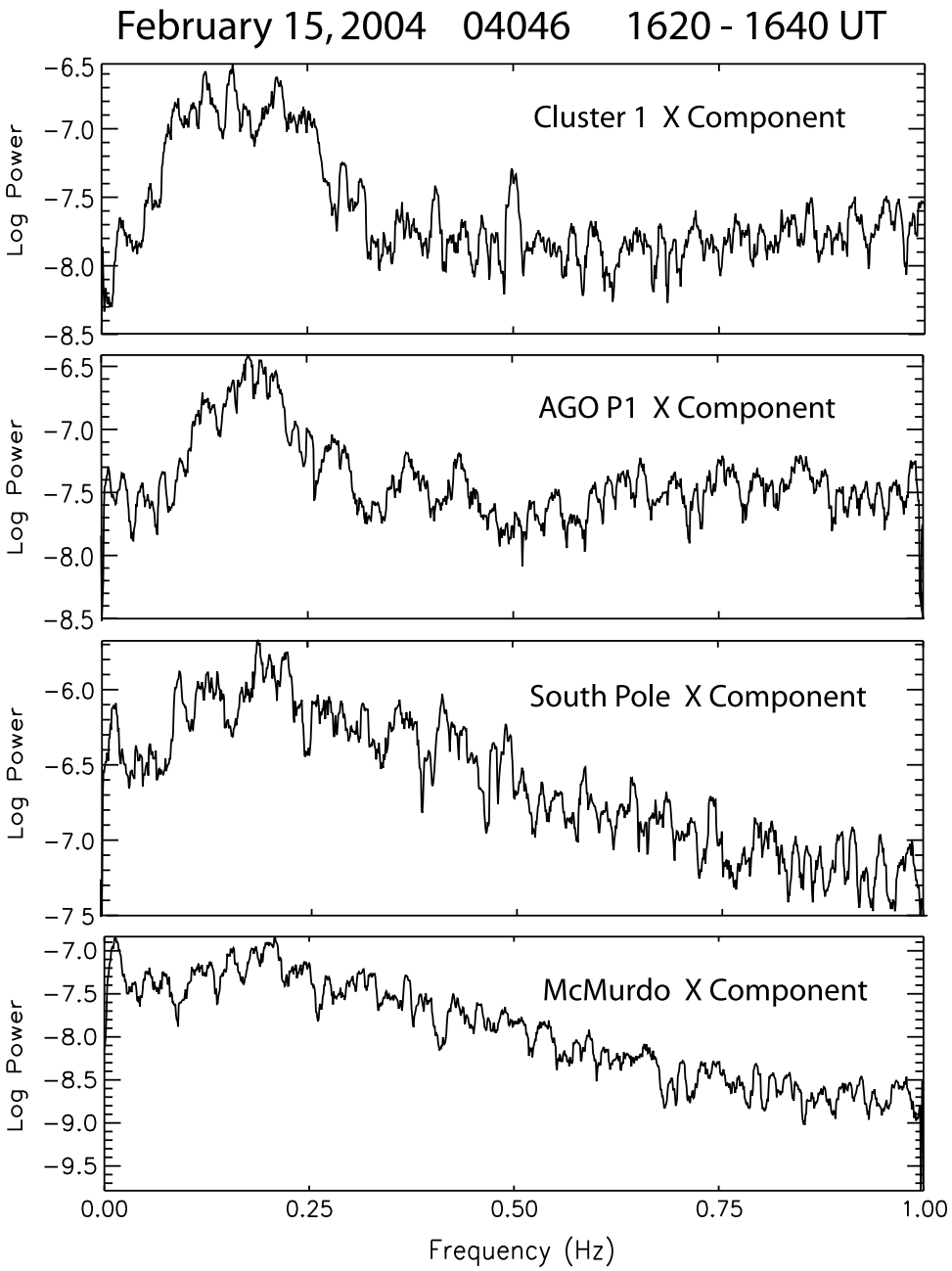

Figure 7. Stacked plots of Fourier spectra of the X component of magnetic field data in field-aligned components (top) from Cluster 1, and of the north-south component of search coil data from AGO P1, South Pole, and McMurdo, Antarctica for the interval 1620 to 1640 UT 15 February 2004.

(CGMLAT 80°). Figure 5 (bottom right) shows the time-shifted OMNI IMF data for the 1600–1800 UT interval on this day (obtained from CDAWEB at http://cdaweb.gsfc.nasa.gov/). By was strongly negative from 1600 to ~1625 UT, and Bz was strongly negative, but with some fluctuations, from ~1625 until 1710 UT.

[20] Figures 6a and 6b, in a format identical to that of Figure 2, show upgoing ions observed by Cluster-1, in this case with considerably higher energy (center energies varying from ~400 eV to ~1 keV), qualitatively consistent with the higher spacecraft altitude. Figures 6c and 6d indicate that waves of very similar frequency (~0.2 Hz) appeared at Cluster-1 and on the ground at AGO P1 between 1600 and 1645 UT, when the Cluster-1 footpoint passed nearby. The waves were again observed at the same time as increased fluxes of upgoing ions (Figure 6b).

[21] Figure 7 shows stacked X-component Fourier spectra, as in Figure 4, from Cluster-1, AGO P1, South Pole Station, and McMurdo, from 1620 to 1640 UT. During this interval South Pole Station and AGO P1 were at ~1300 magnetic local time, and McMurdo was at 0930 MLT. Wave power was enhanced from ~0.1 to 0.25 Hz at all four locations, but only weakly at McMurdo. Although the relative enhancement was largest at AGO P1, nearest to Cluster's footpoint, the absolute power was ~5 times larger at South Pole, located at the footpoint of field lines nearer to the nominal

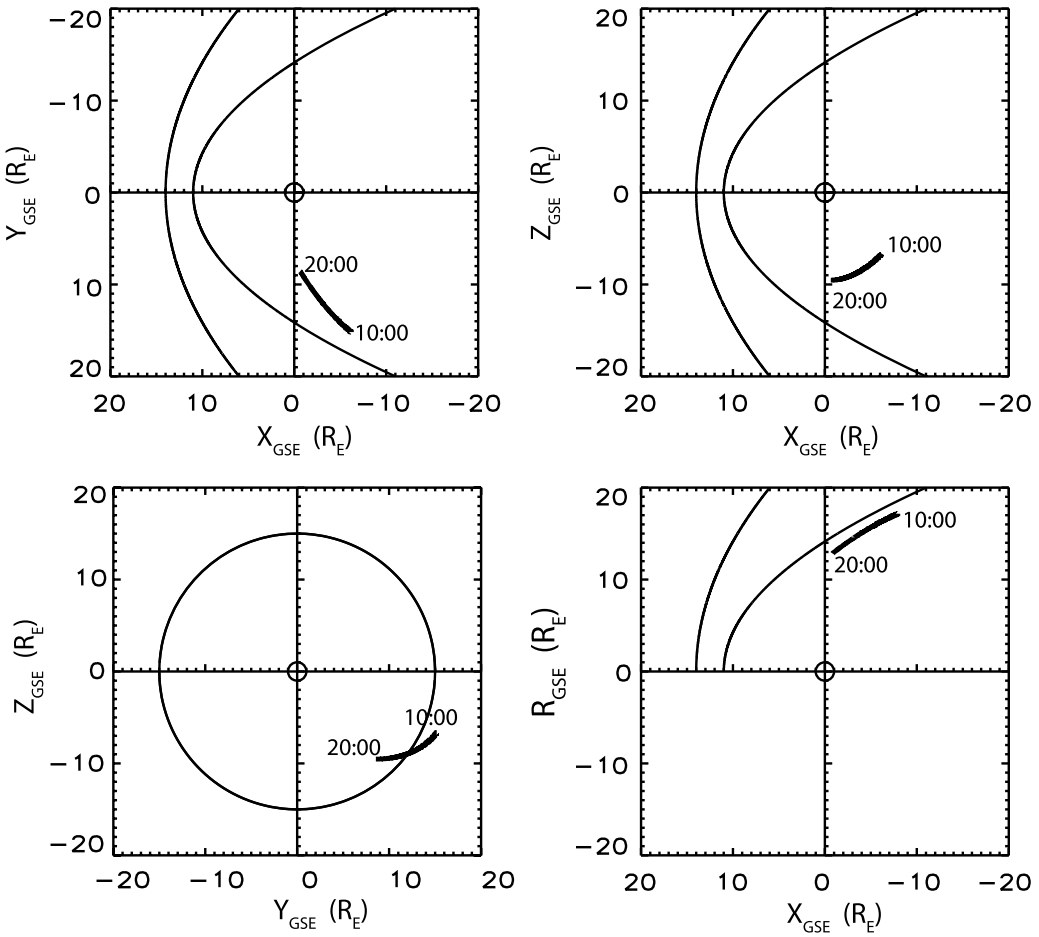

Figure 8. Orbit of the Cluster 1 spacecraft from 1000 to 2000 UT 3 November 2002 (YRDAY 02307). Shown are projections of the orbit in (top left) the GSE X–Y plane, (top right) the GSE X–Z plane, (bottom left) the GSE Y–Z plane, and (bottom right) as a function of GSE X and the distance from the Earth-Sun line. Modeled locations of the bow shock and magnetopause are also shown in each figure.

dayside cusp. In addition, the similarity between ground spectra and Cluster spectra was greater for stations nearer to the spacecraft ground track (AGO P1, then South Pole, then McMurdo).

4. Other Cluster Observations in the High Altitude Plasma Mantle/Lobe

[22] In this section we present observations during two of the longest-duration wave events of the 46 observed during the 2002 and 2003 Cluster tail passages.

4.1. Event 1: 3 November 2002

[23] Figure 8 shows the location of Cluster between 1000 and 2000 UT on this day, as the spacecraft traveled Sunward and Earthward through the southern dusk lobe region (Figure 8a) and toward increasingly large negative Z_{GSE} (Figures 8b and 8c). Figure 8d shows that during this entire 10-h interval, the spacecraft traveled roughly parallel to the nominal magnetopause, but remained within the magnetosphere.

[24] Figures 9a, 9b, and 9c show Fourier spectrograms of all three field-aligned magnetic field components observed by Cluster-1 from 1000 to 2000 UT 3 November 2002 (YRDAY 02307), and Figure 9d shows the total magnetic field. Band-limited wave power was observed during several extended intervals between 1000 and 2000 UT. Representative peak-to-peak amplitudes were ~1.0 nT at 1100 UT and 0.3 nT near 1830 UT. Waves were predominantly transverse, with very little compressional power. Wave activity showed little correlation with compressions of the total field (Figure 9d). Wave occurrences were, however, roughly simultaneous with intervals of southward IMF B_z, as shown in Figure 9e, taken from the time-shifted OMNI data base (see http://cdaweb.gsfc.nasa.gov).

[25] The center wave frequency increased unsteadily from ~0.33 to ~0.55 Hz during this interval, in rough agreement with the increase in |B| shown in Figure 9d, but there was no temporal correlation between wave events and increases in |B|. As shown in Table 2, the normalized frequency $X = \omega/\Omega_p$, was between 0.5 and 0.6 during this 10-h interval. Waves were predominantly transverse, with very little compressional power. The wave amplitude ranged from 0.5 to 2 nT p-p.

[26] Figure 10 shows the ions observed simultaneously with these waves. Figure 10a repeats Figure 9a. Figure 10b is an energy spectrogram of omnidirectional fluxes, and Figure 10c is a pitch angle spectrogram, respectively, of ions

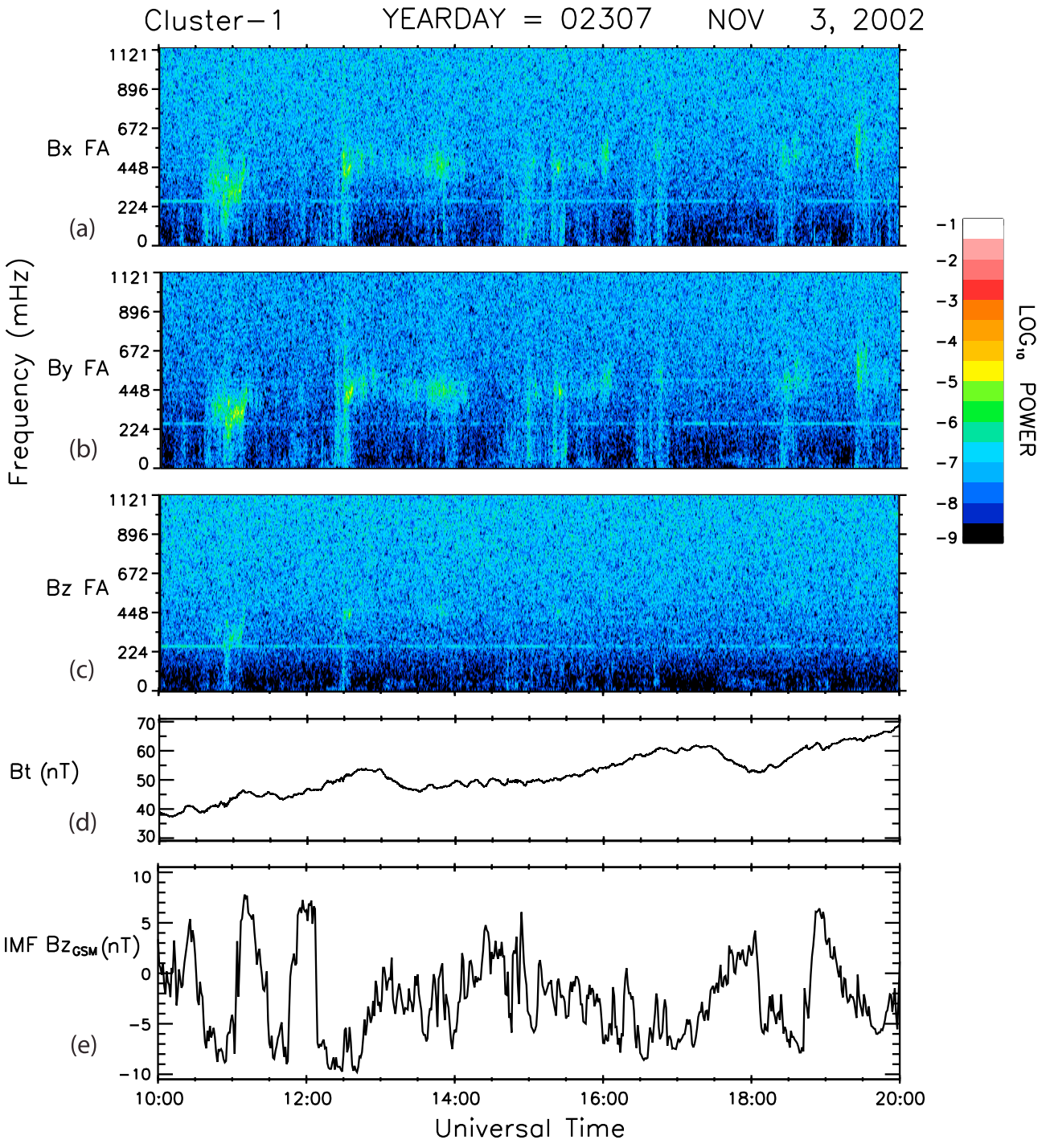

Figure 9. Fourier spectrograms of magnetic field data (a–c) in mean field-aligned coordinates from Cluster 1, (d) plot of the total magnetic field, and (e) plot of the OMNI time-shifted Bz component of the interplanetary magnetic field (IMF) in the GSM coordinate system, from 1000 to 2000 UT 3 November 2002.

measured by the CIS-HIA instrument on Cluster-1. The remaining panels show ion data obtained by the CIS-CODIF instrument on Cluster-1: Figures 10d and 10e show energy spectrograms of omnidirectional H^+ and O^+ fluxes and Figure 10f shows their number density; Figures 10g and 10h show the velocity components of the H^+ and O^+ ion populations, respectively, in the GSM coordinate system, and Figures 10i and 10j show the parallel and perpendicular (to **B**) temperatures of the H^+ and O^+ ion distributions, respectively.

[27] Because the CIS-HIA instrument does not distinguish between ion species, the energy spectrogram in Figure 10b shows two traces: a narrow upper trace and a broader, more intermittent lower trace. The CIS-CODIF spectrograms, in Figures 10d and 10e, show that these two traces correspond to O^+ and H^+ ions, respectively. These show that

Table 2. Approximate Center Frequency and Normalized Frequency $X = \omega/\Omega_p$ of ULF Waves Observed During 3 November 2002

Time (UT)	f (mHz)	X
10:35–11:15	325	0.50
12:20–14:10	450	0.60
14:40–16:10	450	0.57
16:25–16:50	450	0.50
18:15–18:50	450	0.51
19:25–19:50	550	0.55

O^+ ions in a narrow range of modestly varying energies near 1 keV were observed throughout this 10-h interval. Their energy increased when fluxes of lower energy H^+ ions increased by factors of 10–100, and waves occurred only during the most intense of these H^+ intervals (Figure 10f). Figure 10c, a CIS-HIA pitch angle spectrogram of all ion species with energy ≤1 keV, indicates the ion distribution was limited to low pitch angles; that is, the (mostly hydrogen) ions were streaming tailward, parallel to **B**, during the entire 10-h interval. Figures 10g and 10h, from the CIS-CODIF instrument, show that the bulk velocities of H^+ and O^+ ions were very similar, ranging from ∼100 to ∼240 km/s, higher during times of the strongest H^+ fluxes and wave activity, and were oriented predominantly in the $-X_{GSM}$ direction, that is, tailward and flaring outward toward positive Y_{GSM} and negative Z_{GSM}. The large scatter in H^+ velocities seen, for example, near 1800 UT, is a result of the very low count rates at that time.

[28] Figures 10i and 10j show perpendicular and parallel temperatures for H^+ and O^+, respectively, indicating a large temperature anisotropy (∼3) for H^+ but little or none for O^+. (The large variances in temperature in intervals of no wave activity are again due to low count rates. They are primarily due to noise and should be disregarded.)

4.2. Event 2: 25 November 2002

[29] Figure 11 shows the location of Cluster-1 between 0000 and 0600 UT on this day, as the spacecraft again traveled Earthward through the southern dusk lobe region (Figures 11a, 11b, and 11c), in this case much closer to the nominal magnetopause (Figure 11d). Figures 12 and 13 show magnetic field and ion data from Cluster-1, while Figure 14 shows magnetic and electric field data for a shorter time interval from Cluster-4.

[30] Three distinct intervals of magnetic activity are shown in Figure 12. Figure 12a is a Fourier spectrogram of the X-component in mean field-aligned coordinates, as in Figures 9 and 10. The interval from 0000 UT to 0115 UT was dominated by broadband noise that extended from DC to nearly 10 Hz (well above the ∼1.1 Hz upper limit of the spectrogram shown), but also included more intense narrowband wave power near 0.35 Hz. Broadband noise was also dominant from ∼0150 to 0220 UT, but was followed by much more band-limited wave activity from 0220 to 0310 UT near 0.2 Hz, 0.35 Hz, and more weakly near 0.8 Hz. Much weaker and more narrowband wave activity appeared between 0400 and 0520 UT, with peak-to-peak amplitude near 0.4 nT. Similar activity but with larger amplitude was observed during this latter interval at Cluster-3 and Cluster-4 (1.5 nT p-p), which were located respectively 1.0 and 0.8 R_E farther from Earth and roughly 0.5 and 0.4 R_E farther out toward the magnetopause.

[31] Figure 12b shows the wave ellipticity during this event (pixels are black when the wave power was less than 10^{-7} nT^2-Hz). As was the case for all other wave events in this study, the band-limited waves were left-handed (had negative ellipticity) even in the presence of noise, while the broadband noise was randomly polarized. Figure 12c, a plot of the total magnetic field |B|, reveals numerous rapid drops in magnetic field magnitude and generally reduced total field during the intervals of broadband noise but relatively steady |B| values when no broadband waves were observed.

[32] The broadband ULF noise and narrow frequency regions of embedded left-handed polarization shown during two intervals in Figure 12b resemble the observations presented by *Fuselier et al.* [1994] in the dayside magnetosheath. Their Figure 2 shows a similar pattern: modest narrowband increases of left-handed polarized wave power are superposed on an otherwise featureless broadband noise spectrum. That study, one of a set of papers analyzing magnetosheath plasma parameters and their relation to EMIC waves, showed evidence that EMIC waves regulated the local ion temperature anisotropy in the magnetosheath even when broadband turbulence was dominant.

[33] Figures 12d, 12e, and 12f show OMNI time-shifted interplanetary magnetic field and solar wind data for this time interval. A large, positive By component dominated the IMF during each of the three narrowband wave intervals (Figure 12d); the IMF Bz component was significantly smaller but of variable sign (Figure 12e). The two intervals of increased solar wind velocity between 0000 and 0110 and 0200–0315 shown in Figure 12f correlated with intervals of reduced and highly variable total magnetic field (Figure 12c). These increases in the solar wind velocity, combined with a relatively steady solar wind density near 4 cm^{-3} throughout this interval (not shown), resulted in increased solar wind pressure. We infer that this increased Psw compressed the magnetosphere such that the Cluster satellites, located nominally near the magnetopause, would during these times be in the exterior cusp, boundary layer, or magnetosheath. The similarity to the power spectrum shown by *Fuselier et al.* [1994] and the highly variable |B| values (a signature of a magnetosheath region downstream from a quasi-parallel shock [*Engebretson et al.*, 1991; *Fuselier et al.*, 1994]), as well as ion data to be shown in Figure 13 below, provide additional support for this inference.

Figure 10. (a) Fourier spectrogram of the X component of Cluster-1 magnetic field data (as in Figure 9), from 1000 to 2000 UT 3 November 2002. (b and c) Energy spectrogram of omnidirectional fluxes and pitch angle spectrogram, respectively, of ions measured by the CIS-HIA instrument on Cluster-1. The remaining panels show ion data obtained by the CIS-CODIF instrument on Cluster-1: (d and e) show energy spectrograms of omnidirectional H^+ and O^+ fluxes and (f) shows their number density; (g and h) show the vector components of the H^+ and O^+ ion distributions, respectively, in the GSM coordinate system, and (i and j) show the parallel and perpendicular (to **B**) temperatures of the H^+ and O^+ ion distributions, respectively.

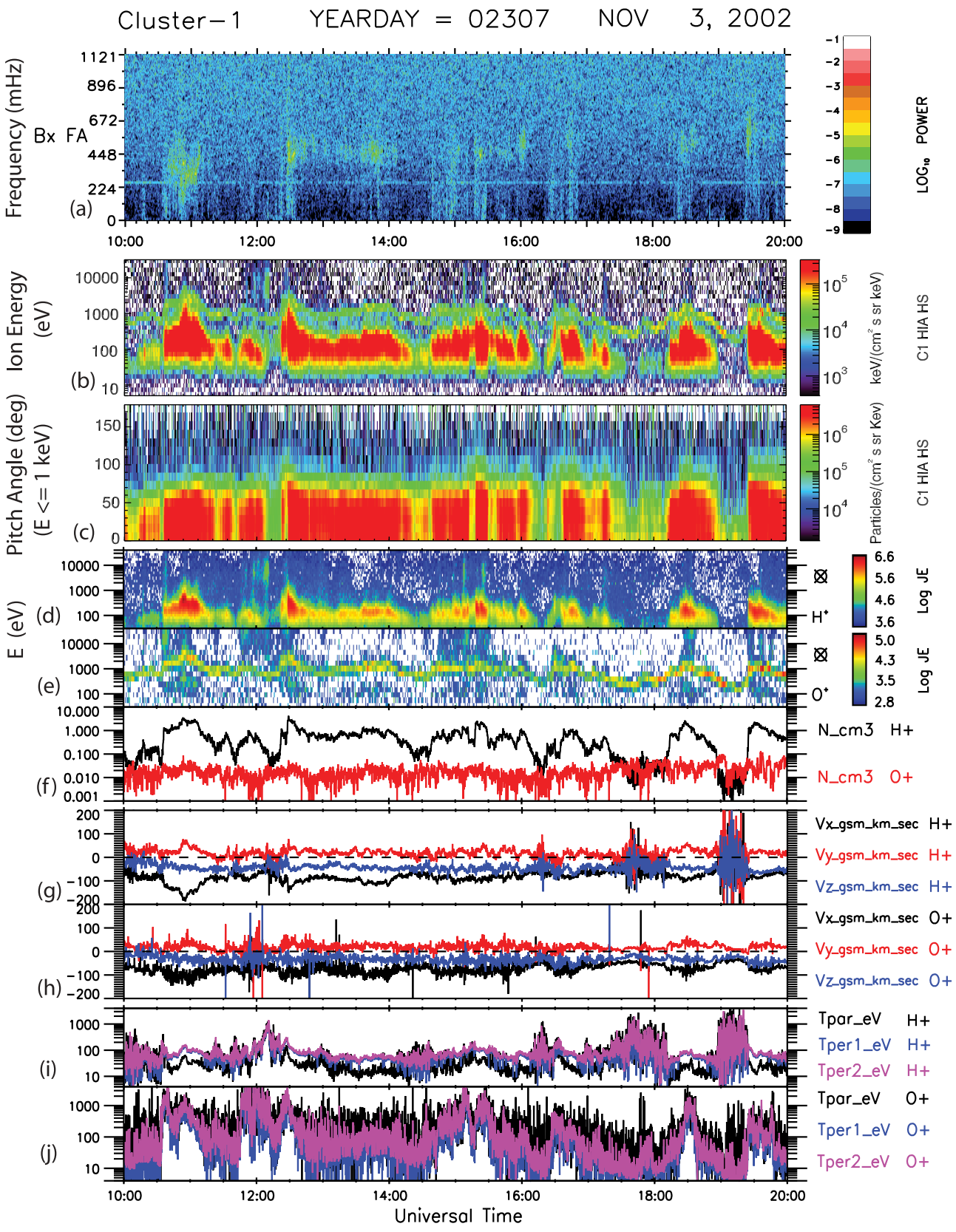
Cluster−1 YEARDAY = 02307 NOV 3, 2002
Frequency (mHz)
Bx FA
(a)
1121
896
672
448
224
0
10:00
12:00
14:00
16:00
18:00
20:00
LOG10 POWER
Ion Energy (eV)
(b)
10000
1000
100
10
C1 HIA HS
keV/(cm2 s sr keV)
Pitch Angle (deg) (E <= 1 keV)
(c)
150
100
50
0
Particles/(cm2 s sr Kev)
E (eV)
(d)
H+
Log JE
(e)
O+
(f)
N_cm3 H+
N_cm3 O+
(g)
Vx_gsm_km_sec H+
Vy_gsm_km_sec H+
Vz_gsm_km_sec H+
(h)
Vx_gsm_km_sec O+
Vy_gsm_km_sec O+
Vz_gsm_km_sec O+
(i)
Tpar_eV H+
Tper1_eV H+
Tper2_eV H+
(j)
Tpar_eV O+
Tper1_eV O+
Tper2_eV O+
Universal Time

Figure 10

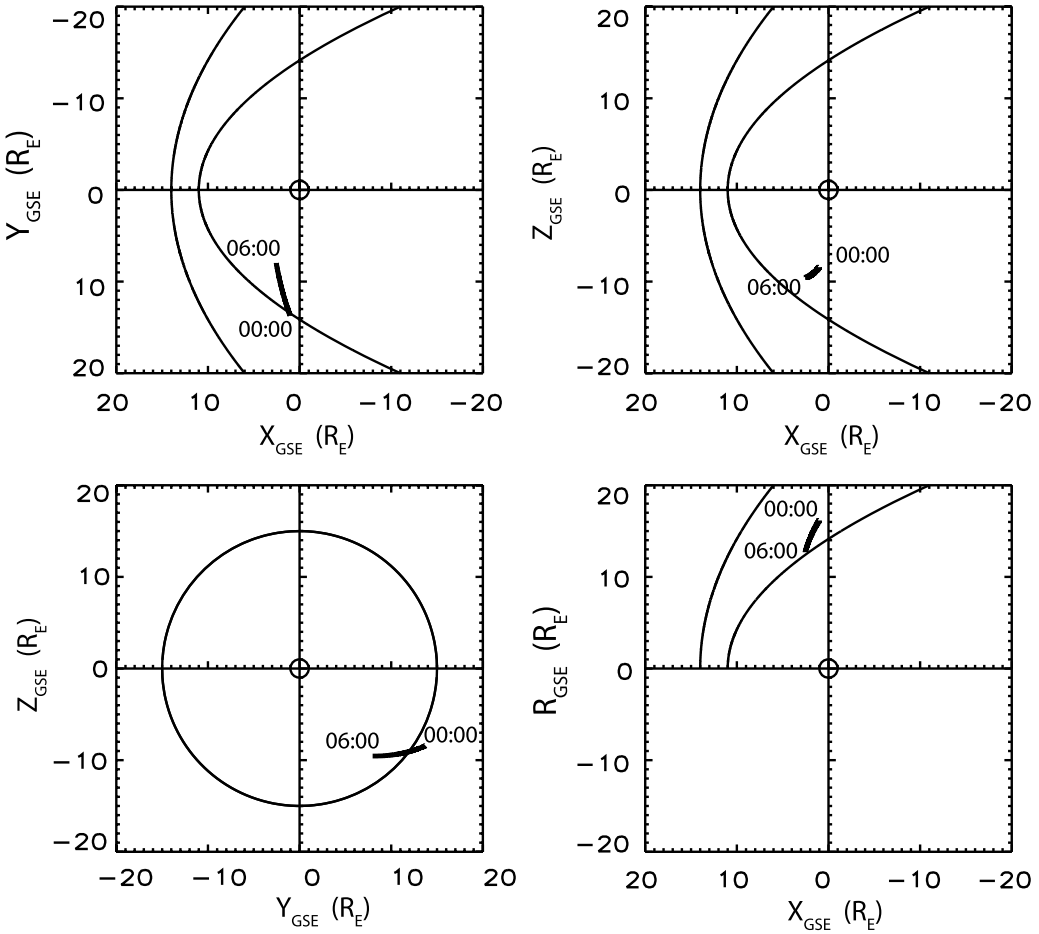

Figure 11. Orbit of the Cluster 1 spacecraft from 0000 to 0600 UT 25 November 2002 (YRDAY 02329). Shown are projections of the orbit in (top left) the GSE X–Y plane, (top right) the GSE X–Z plane, (bottom left) the GSE Y–Z plane, and (bottom right) as a function of GSE Z and the distance from the Earth-Sun line. Modeled locations of the bow shock and magnetopause are also shown.

[34] Figure 13, in a format similar that of Figure 10, repeats the event 2 Fourier spectrogram of the X-component of the magnetic field in mean field-aligned coordinates in Figure 13a, and in subsequent panels displays ion data from the CIS HIA and CODIF instruments for this event. The CIS-HIA energy spectrogram in Figure 13b again shows two traces, corresponding to O^+ and H^+ ions, respectively, and again indicates energization of the O^+ ions during times of significant increases in energy and flux of H^+. Also, as was the case for event 1, Figure 13c indicates that the ion distribution was limited to low pitch angles, streaming tailward parallel to **B**, during the entire interval.

[35] The CIS-CODIF spectrograms, in Figures 13d and 13e, again show that these two traces correspond to O^+ and H^+ ions, respectively. Intense proton fluxes during the two broadband noise intervals (Figure 13d) extended in energy from below 100 eV to 10 keV. In contrast, during the weak wave event between 0400 and 0520 UT, protons were much more narrowly peaked near 100 eV. The energy of the streaming O^+ ions, shown in Figure 13e, also increased by more than a factor of 10 during the broadband noise intervals, and densities of both H^+ and O^+ increased during these times (Figure 13f). (The lower energy O^+ band evident in Figure 13e near 1 keV during the broadband noise intervals is a consequence of instrumental contamination from the large H^+ signal, i.e., a spill-over effect.)

[36] Figures 13g and 13h show that the bulk velocities of H^+ and O^+ ions were very similar after 0330 UT, as was the case for event 1, and were again oriented predominantly tailward along **B**, but the H^+ ions exhibited significantly larger bulk velocity than the O^+ ions during the two broadband noise intervals. The perpendicular and parallel temperatures for H^+ and O^+ shown in Figures 13i and 13j again indicate a large temperature anisotropy ($\sim$3) for H^+ during each interval when narrowband waves were observed, but a reverse anisotropy ($T_{\|} > T_{\perp}$) for O^+. Little or no temperature anisotropy was evident for H^+ during intervals when only broadband noise was observed (e.g., 0000–0030 UT and

Figure 12. Fourier spectrogram of the X component (a) of Cluster-1 magnetic field data and (b) of wave ellipticity, (c) plot of the total magnetic field in nanoTeslas at Cluster-1, (d and e) OMNI time-shifted y and z components of the interplanetary magnetic field (IMF) in the GSM coordinate system, and (f) OMNI time-shifted solar wind velocity, from 0000 to 0600 UT 25 November 2002 (YRDAY 02329).

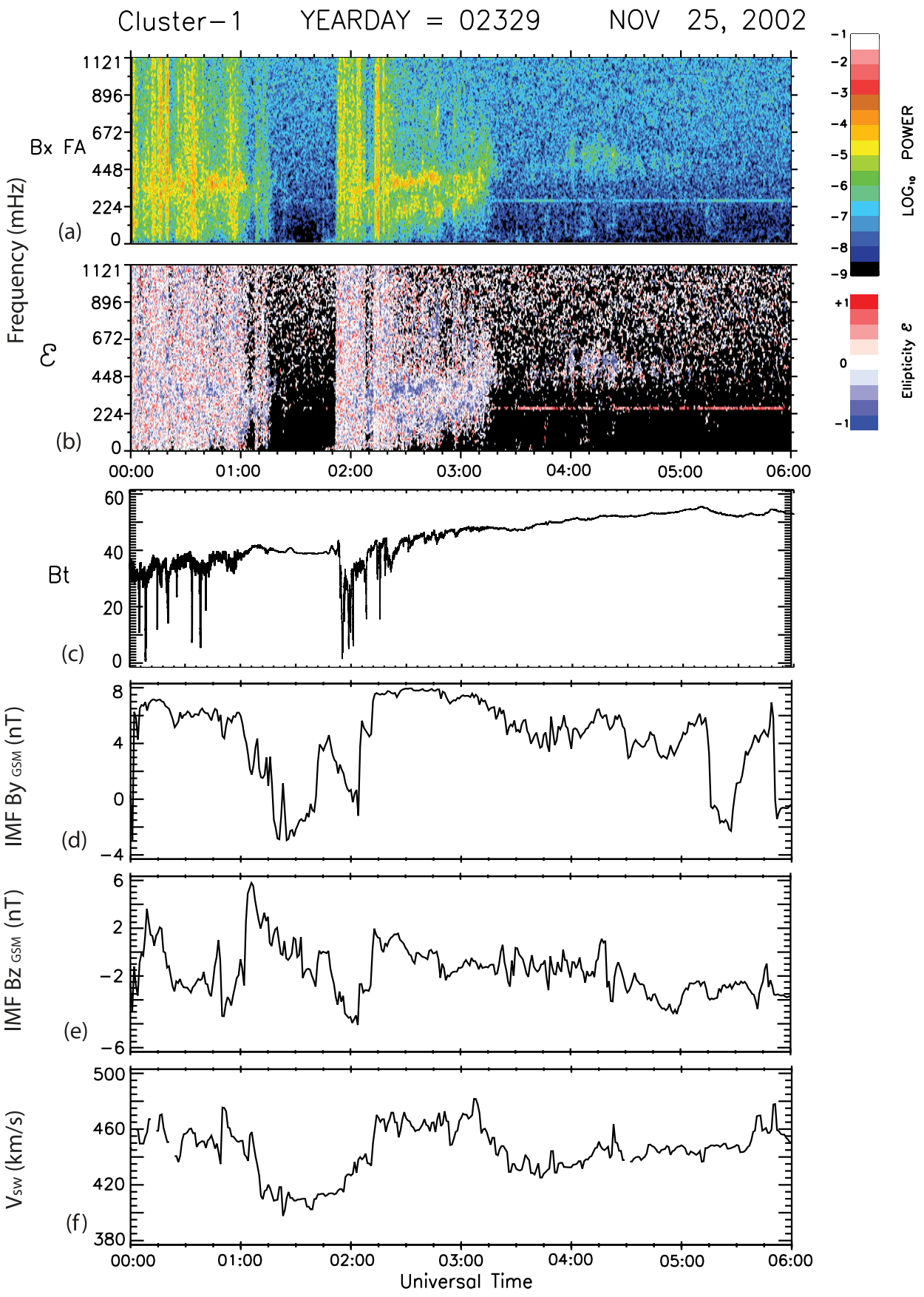
Cluster−1 YEARDAY = 02329 NOV 25, 2002
Bx FA
Frequency (mHz)
(a)
(b)
Bt
(c)
IMF By GSM (nT)
(d)
IMF Bz GSM (nT)
(e)
Vsw (km/s)
(f)
LOG10 POWER
Ellipticity ε
Universal Time
00:00
01:00
02:00
03:00
04:00
05:00
06:00

Figure 12

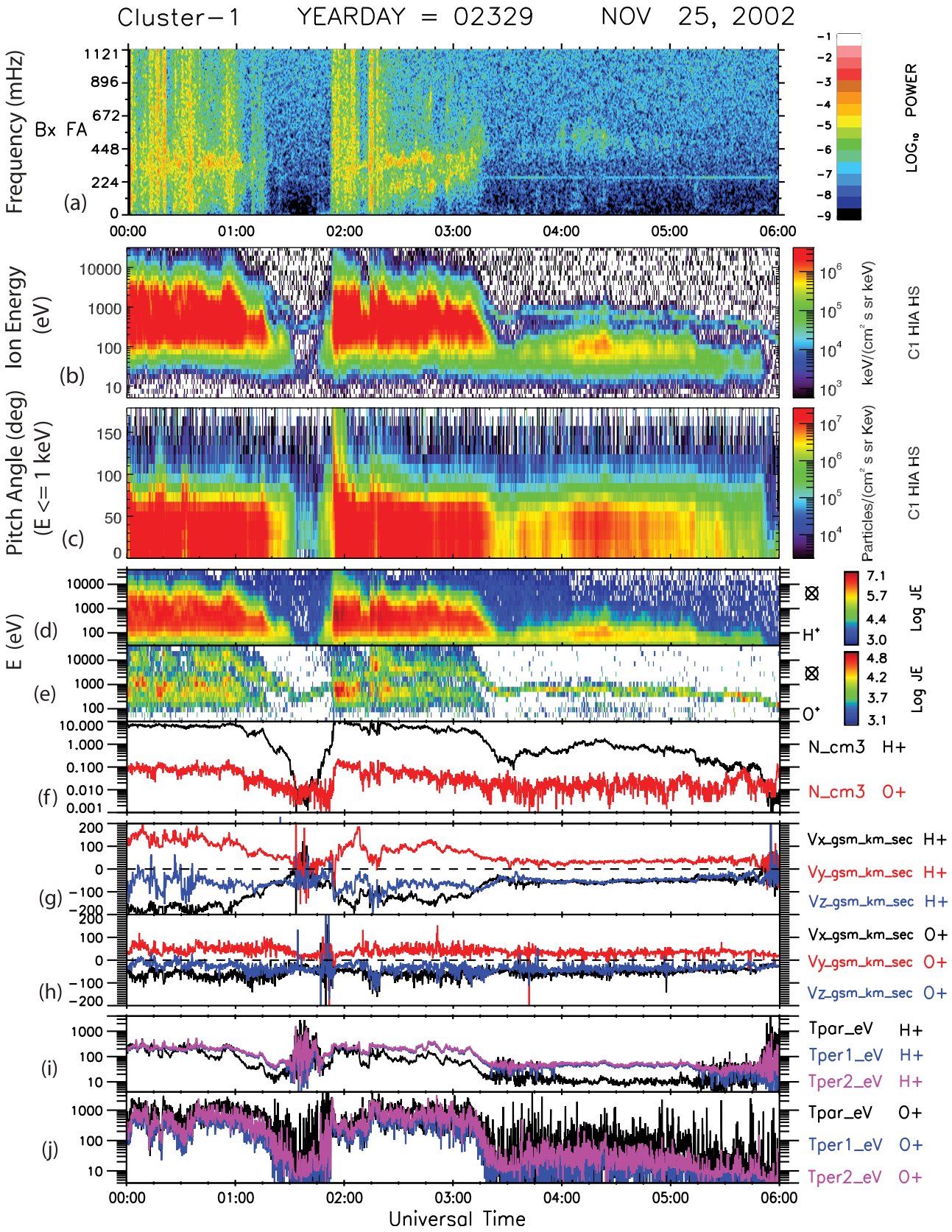

Figure 13. Field-aligned X-component magnetic field spectrogram and ion data from CIS-HIA and CIS-CODIF for the interval 0000–0600 UT 25 November 2002, as in Figure 10.

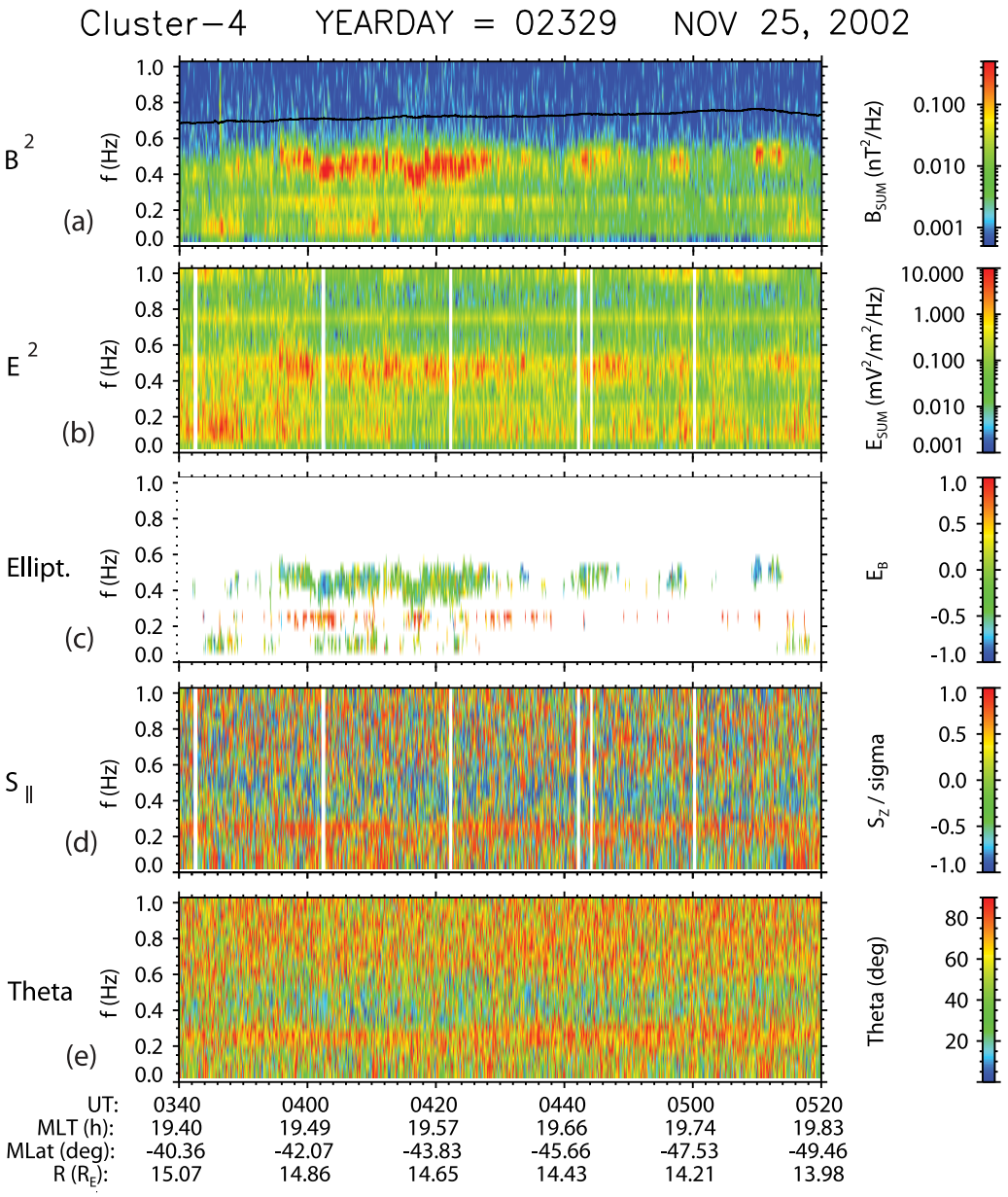

Figure 14. Summed power spectral densities of (a) 3 components of **B** and (b) 2 components of **E**, respectively, measured by Cluster-4. The black line in Figure 14a shows the proton cyclotron frequency. The three lower panels show wave parameters calculated using PRASSADCO software: (c) ellipticity, plotted only when the total magnetic power spectral density was larger than 0.05 nT^2/Hz, (d) Poynting vector direction, and (e) propagation angle relative to **B**.

0155–0210 UT). Both the significantly larger H^+ bulk velocity and number density during the intervals of broadband noise are consistent with our inference that Cluster-1 had most likely crossed into the high altitude cusp region and/or magnetosheath during these times.

[37] As noted above, Cluster-3 and -4 observed similar but much more intense narrowband waves from 0340 to 0520 UT on this day. Waves at both Cluster-3 and -4 during this interval were associated with H^+ densities 2–3 times higher than those observed at Cluster-1. Figure 14 shows wave parameters calculated from observed B and E measurements at Cluster-4 for this event. Figures 14a and 14b show summed power spectral densities of 3 components of **B** and 2 components of **E**, respectively. The black line shows the local proton cyclotron frequency. Waves are again evident between 0.4 and 0.5 Hz, as in panel 1 of Figure 13. Figure 14c shows the color-coded ellipticity of the magnetic field using the singular value decomposition (SVD) analysis of *Santolík et al.* [2003], plotted only when the total magnetic power spectral density was larger than 0.05 nT^2/Hz. The waves were once again predominantly left handed (green to blue color), but with some evidence of more linear polarization as well. Figure 14d shows an estimation of the component of the Poynting vector parallel to the average magnetic field $\mathbf{B}_0$ normalized by its standard deviation using the 5*5 spectral matrices [*Santolík et al.*, 2001]: the Poynting vector for

waves between 0.4 and 0.5 Hz was opposite to $\mathbf{B}_0$ (blue color), and hence again directed Earthward. The right-handed polarization and field-aligned Poynting flux seen around 0.25 Hz are artifacts of satellite spin. Figure 14e shows the angle θ between the wave vector and the background magnetic field. The small but nonzero propagation angles associated with the waves (from 0 to 45°) indicate that these waves propagate obliquely and are guided along $\mathbf{B}_0$, as reviewed in section 6.3.

5. Statistical Study

[38] In order to better understand the range of locations, geomagnetic conditions, and plasma parameters associated with these waves, we surveyed all Cluster data during 2 years of Cluster's passage through the magnetotail, with orbital precession covering dawn to dusk on Earth's night side: June through December of 2002 and June through November of 2003. CIS spectrograms were reviewed to confirm the association of these waves with both H^+ and O^+ ions streaming tailward. A total of 46 narrowband wave events were identified on 29 days: 16 of these had contiguous broadband noise events, and 30 had no contiguous broadband events. Intervals dominated by broadband noise and evidently outside the magnetopause, such as the first two intervals in event 2, were not counted, even though the latter 2/3 of the second event might be considered relatively narrowband.

5.1. Locations of Waves

[39] The locations of all the wave events identified in this study are shown in Figure 15. In order to provide context for these events, we first show the Cluster orbits during the time of this study. Figures 15a and 15b, based on data from the NASA SSCweb utility (see http://sscweb.gsfc.nasa.gov/cgi-bin/sscweb/Locator_graphics.cgi), show the precession of the elliptical orbits of the Cluster spacecraft during the 2002 tail season (days 152 to 334); the plot for the 2003 tail season is very similar. Figure 15a shows the projection of the orbits onto the GSE XY plane, and Figure 15b shows a similar projection onto the GSE XZ plane. The perigee of each orbit, at $\sim$4 R_E, occurs at near-equatorial latitudes at dayside local times.

[40] Figures 15c, 15d, 15e, and 15f show the positions of Cluster during times Pc 1–2 waves were observed poleward and/or tailward of the cusp during the 2002 and 2003 tail seasons. Events with durations under 5 min have been extended to 5 min in each panel in order to make them more visible. Figure 15c shows that these wave events had a distinctive distribution in local time. No events were observed between 2100 and 0200 local time. Although events were distributed widely and approximately symmetrically across the noon-midnight meridian, their X_{GSE} position was largest near local noon and transitioned to negative values as $|Y_{GSE}|$ increased. Figure 15d shows that all events were located at $|Z_{GSE}| > 4$ R_E, with most events having $|Z_{GSE}| > 7$ R_E. The Cluster orbit did not reach to $Z_{GSE} > 7.5$ R_E or $Z_{GSE} < -10.5$ R_E, however, so the upper range of wave events in $|Z_{GSE}|$ cannot yet be determined. Figure 15e, a view from the Sun, reveals a strongly asymmetric distribution of wave events in the GSE YZ plane. Most events occurred in the southern postnoon sector, with a smaller concentration in the northern prenoon sector. Finally, Figure 15f, a plot of the distance from the Sun-Earth line, $R = (Y_{GSE}^2 + Z_{GSE}^2)^{1/2}$, vs. X_{GSE}, shows that, as was the case for the two events shown in section 4, all wave events were concentrated near or inside the mantle/lobe magnetopause boundary.

[41] In order to further examine the relation between these Pc 1–2 waves and the streaming H^+ and O^+ ions observed in all cases with them, we also identified all the time intervals during the 2002 and 2003 tail seasons when streaming H^+ and O^+ ions, with energies similar to those of the wave events, were both identified (Figure 16) in the CIS summary ion spectrograms. Comparison of Figures 16a and 16b with Figures 15c and 15d, respectively, shows that Pc 1–2 waves did not occur far from the magnetopause, or far down the tail, even though streaming ions were observed there. The absence of waves in these regions may be attributable to the lower plasma beta values expected in the tail lobe nearer to the tail midplane (see, for example, the north-south profiles of B and ion density in Figure 1 of *Lui* [1987]). *Rosenbauer et al.* [1975] were the first to note that the ion density in the plasma mantle tended to decrease gradually with depth inside the magnetopause. Calculation of beta for several of these extended passes did in fact show a decline in beta as the Cluster spacecraft traveled inward through the tail lobe from the mantle toward the plasma sheet.

[42] Within the dayside magnetosphere, the occurrence of EMIC waves is greatest at high L values, i.e., in regions closest to the magnetosheath [*Anderson et al.*, 1992a, 1992b]. This spatial pattern can be attributed, in part, to the fact that fast mode compressions are damped as they propagate into the magnetosphere from the magnetopause, and compressions are known to increase the occurrence of dayside EMIC waves [*Anderson and Hamilton*, 1993]. The occurrence of mantle waves is controlled primarily by the presence of elevated levels of streaming ions (as shown for example in Figures 10 and 13). The data shown in Figure 9, however, admits the possibility that compressions, both gradual and more short term, may play a secondary role in contributing to the instability, and such compressions may thus provide an additional reason why mantle waves are observed only near the magnetopause.

5.2. Wave and Plasma Properties

[43] For each of the 46 wave events, we recorded the observed wave frequency, magnetic field magnitude |B|, and normalized wave frequency $X = \omega/\Omega_p$. Events were considered separate if they were spaced 12 min or more apart. We also recorded the plasma beta and the total ion density in the

Figure 15. Plots of the Cluster orbits during times Pc 1–2 waves were observed during the 2002 and 2003 Cluster tail passages. (a and b) All Cluster orbits (in GSE coordinates) during the 2002 tail season (day 152 to day 334), projected onto the XY plane and XZ plane, respectively. (c, d, and e) Cluster positions during times Pc 1–2 waves were observed during the 2002 and 2003 Cluster tail seasons projected onto the XY, XZ, and YZ plane, respectively. (f) A projection of the distance from the Sun-Earth line, $R = (Y_{GSE}^2 + Z_{GSE}^2)^{1/2}$, vs. X_{GSE}. Events with durations under 5 min have been extended to 5 min on the plot to make them more visible.

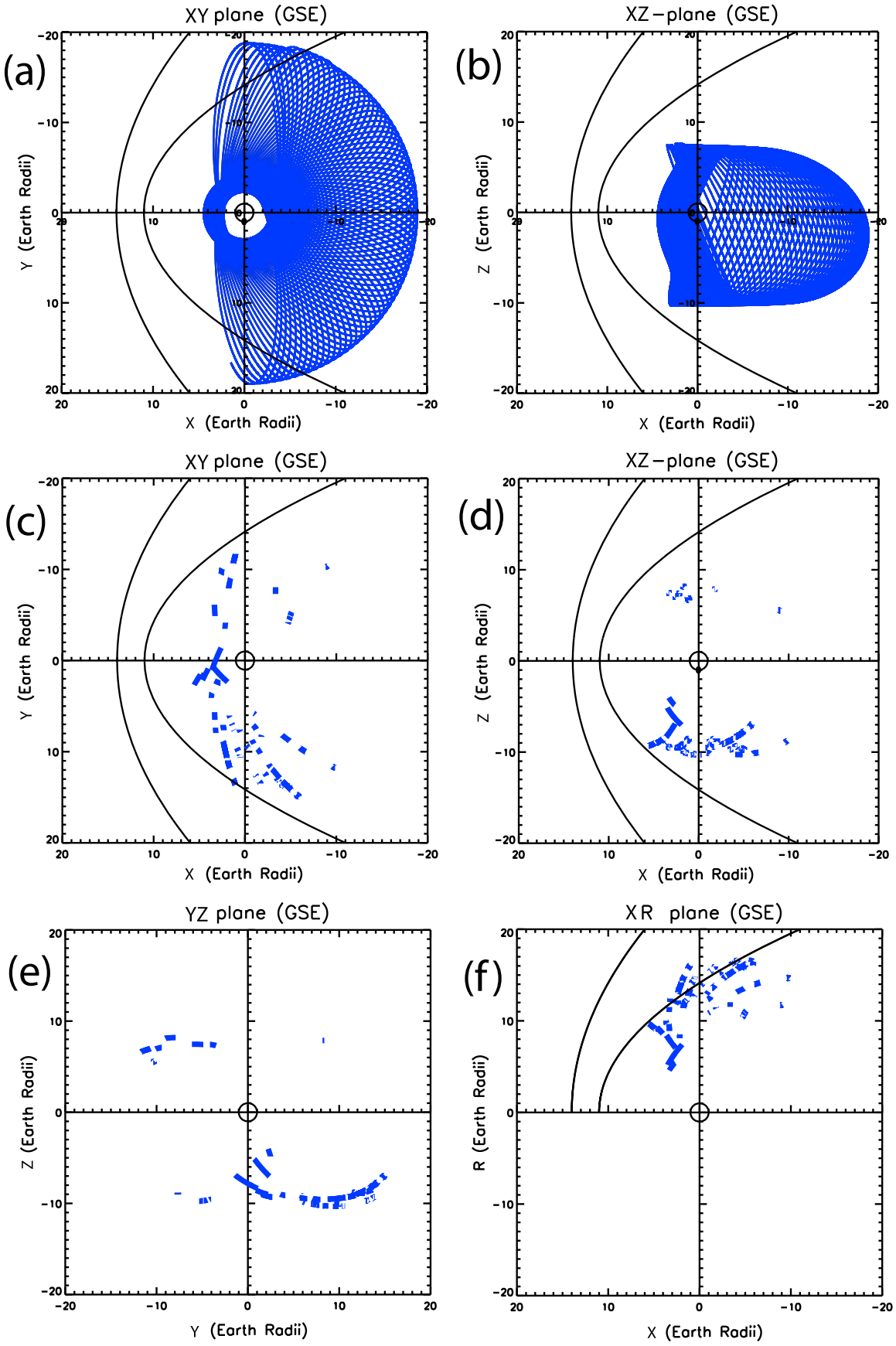
(a)
XY plane (GSE)
Y (Earth Radii)
X (Earth Radii)
(b)
XZ−plane (GSE)
Z (Earth Radii)
X (Earth Radii)
(c)
XY plane (GSE)
Y (Earth Radii)
X (Earth Radii)
(d)
XZ−plane (GSE)
Z (Earth Radii)
X (Earth Radii)
(e)
YZ plane (GSE)
Z (Earth Radii)
Y (Earth Radii)
(f)
XR plane (GSE)
R (Earth Radii)
X (Earth Radii)

Figure 15

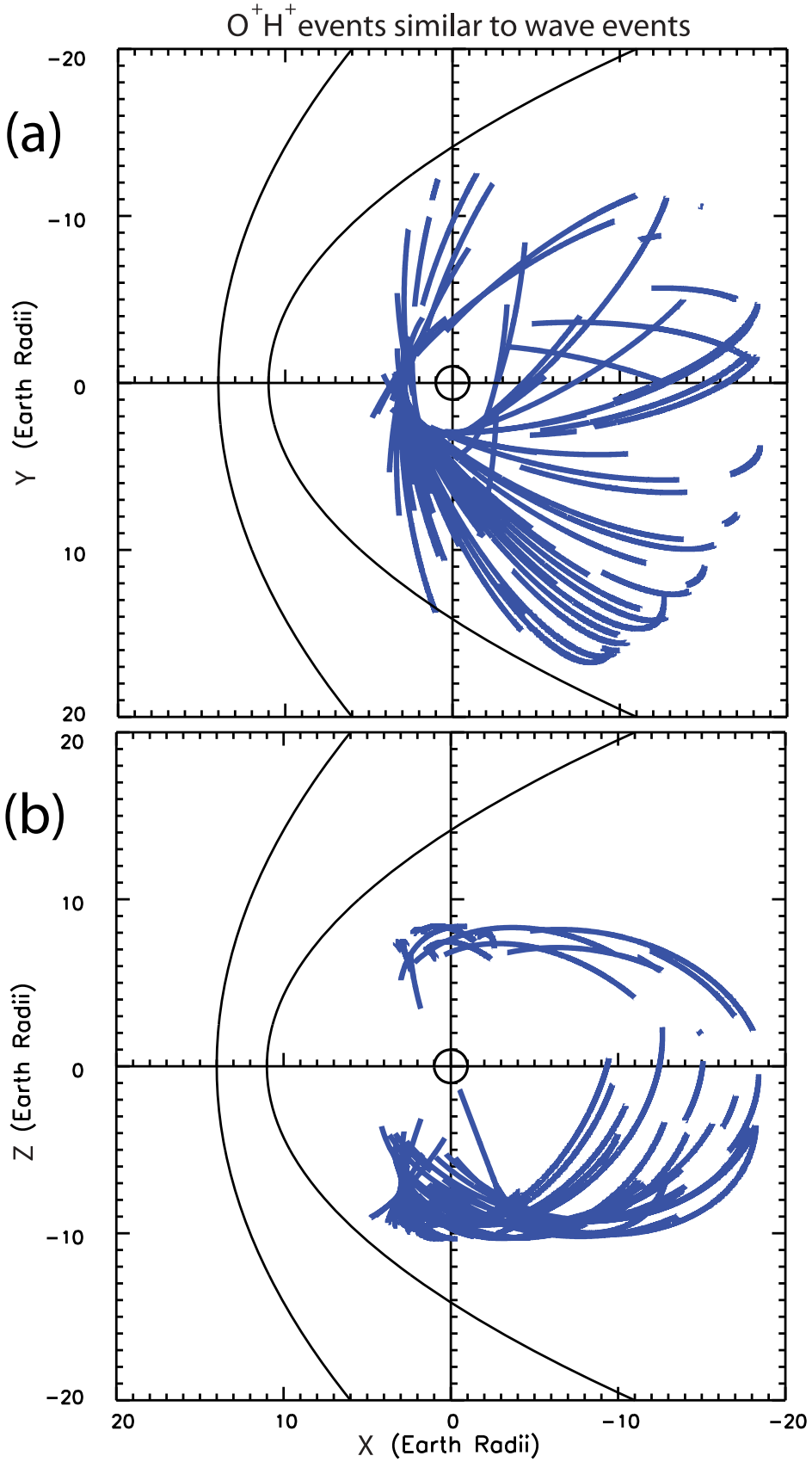

Figure 16. Locations of events during the 2002 and 2003 tail seasons when streaming H^+ and O^+ ions, with energies similar to those observed during Pc 1–2 wave events, were both identified in Cluster data. (a and b) Cluster positions projected onto the GSE XY and XZ planes, respectively.

Table 3. Values of Plasma and Wave Parameters During ULF Wave Events in This Study[a]

Parameter	Average	Std. Deviation	Minimum	Maximum
Ion density (cm^{-3})				
Narrowband Waves	1.46	1.69	0.15	8.0
Contiguous to BBD	2.89	2.19	0.60	8.0
Non-contiguous	0.78	0.72	0.15	3.0
Broadband Noise	14.4	16.4	2.0	70
Quiet Intervals	0.27	0.35	0.03	2.0
Ion beta	0.020	0.021	0.001	0.101
H^+ energy (eV)	192	94	70	400
Center Frequency (Hz)	0.53	0.14	0.25	0.9
Norm. Cent. Freq. $X = \omega/\Omega_p$	0.58	0.11	0.11	0.68

[a]Ion densities are taken from intervals of narrowband waves, contiguous broadband noise intervals, and contiguous quiet intervals.

energy range from ~20 eV to ~38 keV recorded by the CIS CODIF instrument (including both H^+ and O^+) during wave intervals, during the quiet times preceding and following them, and during intervals of temporally contiguous broadband noise (if present).

[44] Table 3 shows the values of plasma and wave parameters during the Pc 1–2 wave events identified in this study. Densities are shown for narrowband wave events (lines 1–3), contiguous broadband events (line 4), and contiguous times with no wave activity (line 5). All other lines show values during narrowband wave intervals. Narrowband wave events are further broken down into events contiguous to broadband noise intervals (we infer that the Cluster spacecraft were nearer to the exterior cusp, boundary layer, or magnetosheath during these times) and events not immediately preceded or followed by broadband noise. That is, assuming that broadband noise intervals occurred during times Cluster was located in the exterior cusp, boundary layer, or magnetosheath, these two classes of wave events may provide some separation by proximity to the magnetopause.

[45] The ion density showed considerable scatter during each category of events, with standard deviations equal to or larger than the average value, but the average densities were an order of magnitude larger during broadband noise events than during narrowband events, and were a further factor of ~5 lower during intervals with no wave activity contiguous to narrowband wave intervals. A comparison of lines 3 and 4 shows that the average ion density was roughly 3 times larger during "contiguous" wave intervals that were presumably near the magnetopause than during "noncontiguous" intervals.

[46] The values of ion beta shown in Figure 17 show a similar pattern. This figure shows the normalized occurrence distribution of ion beta during wave events with and without contiguous broadband noise intervals. Comparison of Figure 17 (top) and 17 (bottom) suggests that although there is a large region of overlap between the beta values for these two sets of events, events with contiguous noise (which we interpret as occurring near the magnetopause boundary) tend to have higher beta values. The average beta value for the upper distribution was 0.028 ± 0.024, while that for the lower distribution was 0.011 ± 0.010. These density and beta dependences are again consistent with earlier observations in the plasma mantle [*Rosenbauer et al.*, 1975; *Lui*, 1987], and are consistent with the high beta and density values in the magnetosheath adjacent to the magnetopause [*Fuselier et al.*, 1994].

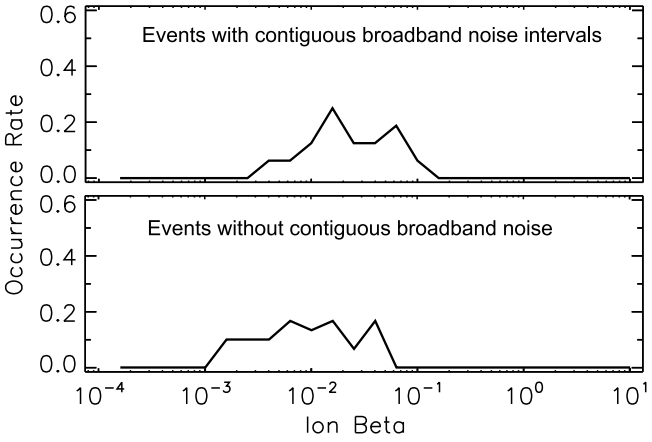

Figure 17. Normalized occurrence distributions of ion beta during Pc 1–2 mantle wave events. (top) Ion beta during events when broadband noise was observed immediately before or after narrowband wave events. (bottom) Ion beta during events when no ULF activity was observed immediately before or after narrowband wave events.

[47] The remaining parameters in Table 3 exhibited considerably less variation. The proton energy distribution, although often broad, was in the range from one to a few hundred eV reported by earlier observers. The observed frequencies varied by less than a factor of 4, from 0.25 to 0.9 Hz. The normalized frequencies, $X = \omega/\Omega_p$, however, exhibited somewhat more variation, which we believe to be an artifact of the propagation of the waves. Figure 18, a plot of X as a function of radial distance from Earth, shows a clustering of X values between 0.45 and 0.7 at large radial distances, but also four lower values, all at low to intermediate radial distances. Because of our observations of waves with similar or identical frequencies on the ground at the magnetic footpoint of Cluster's orbit, and consistent with our observations that the Poynting vector of these waves is field-

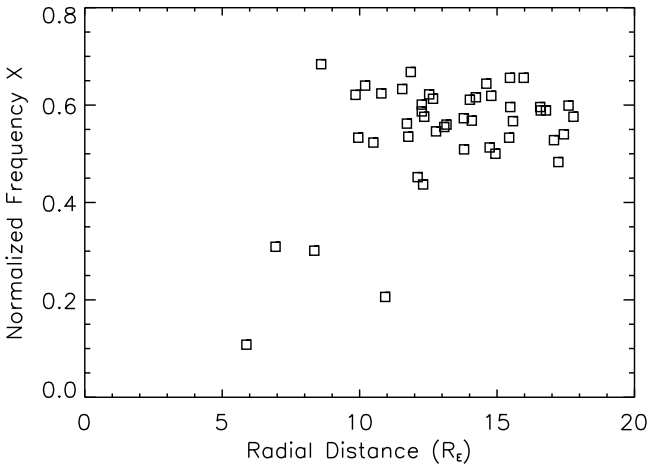

Figure 18. Distribution of the normalized wave frequency $X = \omega/\Omega_p$ vs radial distance from Earth for the wave events identified in this study.

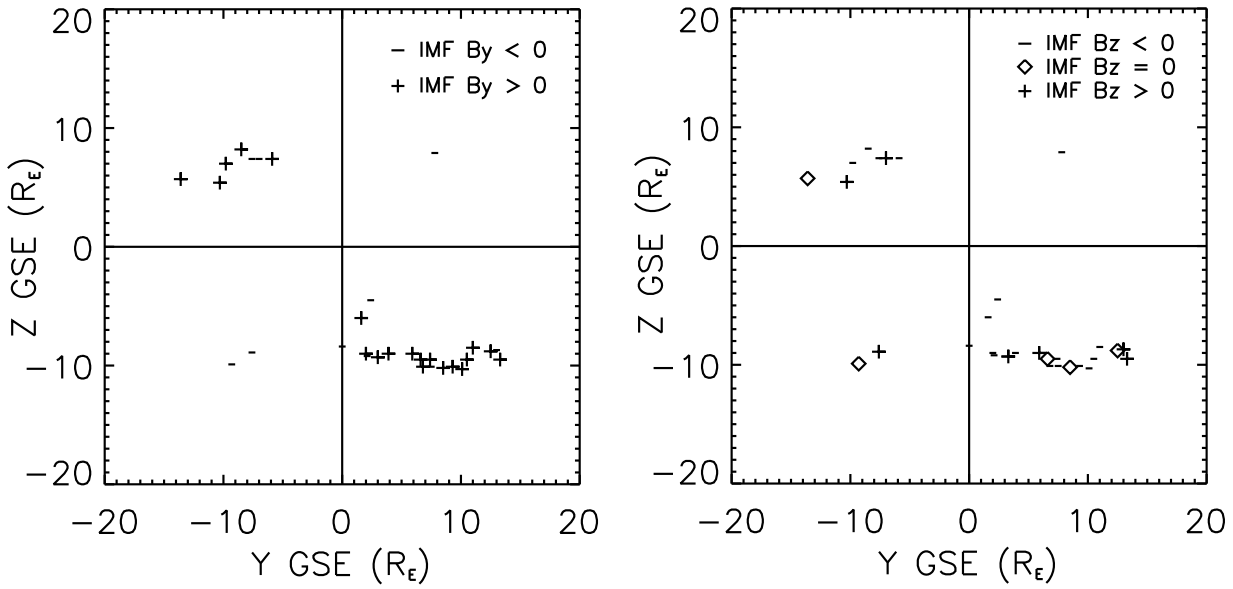

Figure 19. Location of wave events, projected onto the GSE YZ plane. Events are sorted by the polarity of the (left) By component and (right) Bz component of the interplanetary magnetic field.

aligned and Earth-directed, we interpret this figure as suggesting that most of the observed waves are generated at radial distances >8 R_E, and at normalized frequencies between 0.45 and 0.7.

[48] Support for this interpretation also comes from an analysis of the location of the four low-X events. Two of these occurred within 1 h of local magnetic noon (at 1302 and 1141 MLT, in the dayside portion of the plasma mantle), one occurred near dawn (0650 MLT), and one occurred postdusk (1955 MLT). All but the one event near 1302 MLT were observed at very high magnetic latitude (>60°). Only 5 of the other 42 events occurred at |MLAT| > 60 degrees. One of these, with X = 0.452, was at 0630 MLT. The other four (with X = 0.622, 0.576, 0.535, and 0.640) were at postdusk local times. Although the |MLAT| value does not produce a total separation between the events with X above and below 0.35, the observed pattern appears to be consistent with our inference that the waves observed during these four "low-X" events may have originated in more distant regions with lower **B** and propagated Earthward to the satellite's location.

5.3. Solar wind, IMF, and Geomagnetic Conditions

[49] Nearly all of the events occurred during the main or recovery phase of (mostly moderate) magnetic storms. The magnetic indices and standard deviations during the events were as follows: Kp = 3.4 ± 1.0; Dst = −24 ± 29; and AE = 300 ± 170. Roughly one third of the events occurred during main phase, another third during the first day of the recovery phase, and the remaining third during minor intensifications (decreases in Dst) during the later recovery phase.

[50] Figure 19 shows the location of events, as in Figure 15e, as a function of the sign of IMF By and IMF Bz. Nearly 2/3 of the wave events occurred during positive By conditions (left panel), and were observed only in the southern dusk quadrant (most often) or in the northern dawn quadrant. The few wave events occurring when IMF By <0 were observed in all four quadrants, but only such waves were observed in the southern dawn and northern dusk. No pattern of quadrant dependence on IMF Bz values is evident in the right panel.

6. Discussion

6.1. Plasma Origin

[51] As we have shown in panel 3 of Figure 15 and in Figure 19, Pc 1–2 waves in the plasma mantle (in every case associated with streaming H^+ and O^+ ions) have a spatial distribution that is skewed in the GSE Y–Z plane, with events located predominantly in the southern dusk quadrant, and with most of the remainder in the northern dawn quadrant. In their survey of O^+ ion transport in the cusp and lobe regions, *Liao et al.* [2010] also found an asymmetric occurrence pattern of streaming ions in the GSE Y–Z plane, similar to that shown here. They cited *Gosling et al.* [1985], who attributed a similar asymmetry in lobe plasma densities to solar wind particles entering preferentially on the more locally "open" sides of the geomagnetic tail. That the majority of the events were observed in the southern hemisphere may also reflect the fact that Cluster's orbit extended to larger negative Z_{GSE} than positive Z_{GSE}, as shown in Figure 15b.

[52] Because the wave events reported here are statistically associated with greatly increased densities of streaming protons and with either negative IMF Bz or large IMF By components, and are located on field lines (Figure 15f) that would map to near-cusp locations at which reconnection could occur and solar wind/magnetosheath ions could enter Earth's magnetosphere, a correlation to IMF orientations favorable to reconnection appears reasonable. Further supporting the link to reconnection, *Knipp et al.* [2011] found, in a recent analysis of DMSP F-15 data, a pattern of very large high-latitude Poynting fluxes associated with intervals of large IMF By, and subsequent modeling by *Li et al.* [2011] linked such large IMF By intervals with magnetic reconnection at the high-latitude cusps. *Knipp et al.* [2011] also noted that despite their significant geomagnetic activity

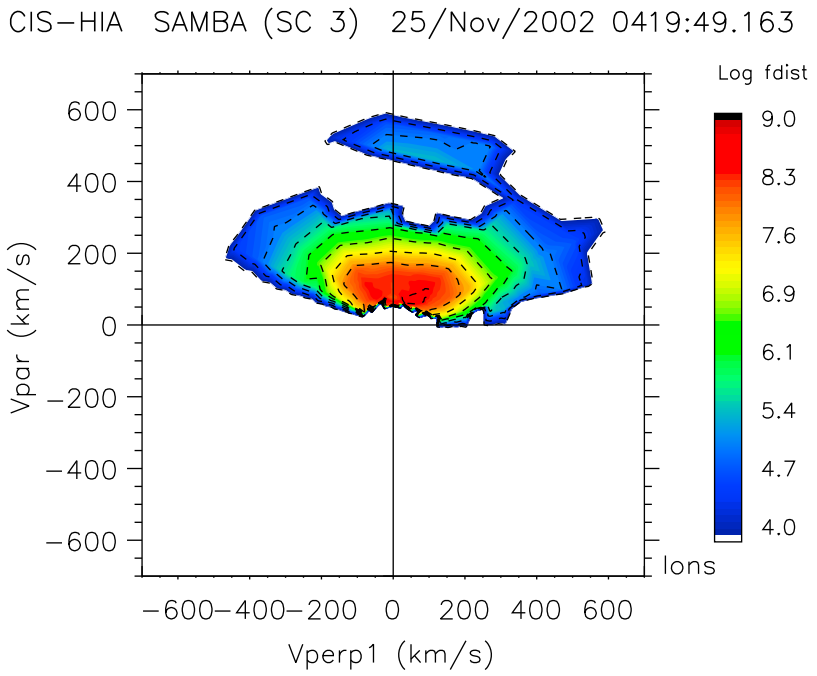

Figure 20. Ion distribution observed by the CIS-HIA instrument on Cluster-3 averaged over a 2-minute interval near 0420 UT 25 November 2002. The color-coded ion phase space density is shown as a function of velocity along the magnetic field direction (vertical axis, with B positive upward) and perpendicular to it (horizontal axis), averaged over 10 distributions (available every 12 s) beginning at 0419:49.163 UT. Contours of the logarithm of the phase space density (in units of s^3/cm^6) are indicated in each panel, two per decade.

at high latitudes, such intervals do not have prominent signatures in geomagnetic storm indices.

6.2. Instability Analysis

[53] As part of an earlier study of Pc 1–2 waves in the mantle based on Polar satellite observations, *Engebretson et al.* [2005] performed an instability analysis of the ions observed at 7.8 R_E based on the temperature anisotropy—beta relationship developed by *Gary et al.* [1995]. They found that the ions observed locally were not unstable to the ion cyclotron instability, but that similar distributions at higher altitudes (near 14 R_E) could be reasonably inferred to be unstable.

[54] Figure 20 shows a cut of the ion distribution function in the $V_{||} - V_{\perp}$ plane near 0420 UT 25 November 2002, based on data from the CIS-HIA instrument on Cluster-3. Because this instrument does not distinguish between ion species, it shows two peaks. The lower $V_{||}$ population (below 400 km/s) is H^+, and the higher $V_{||}$ population is O^+. The reason that the O^+ population appears to have higher velocity (and be more energetic) in HIA data (which does not resolve mass and thus assumes all ions are protons) is simply that the instrument measures the total kinetic energy ($0.5\ mv^2$); i.e., the apparent velocity and energy are mass dependent. The H^+ contours in this figure closely resemble the distribution shown in Figure 9 of *Rosenbauer et al.* [1975], showing both the offset center of the distribution (tailward along **B**) and the large temperature anisotropy ($T_{\perp} > T_{||}$).

[55] Using the WHAMP (Waves in Homogeneous, Anisotropic Multi-component Plasmas) code [*Rönnmark*, 1982, 1984], we performed wave instability calculations relevant to plasma conditions during the period 0435–0515 UT for Cluster 4 on 25 November 2002. The WHAMP code is a linear wave code used to obtain dispersion relations in a homogeneous, multispecies plasma. The distribution functions assumed for the various species are a combination of bi-Maxwellian distributions with the possibility of relative drift along the magnetic field direction. As such, the code can be used to address beam instabilities, anisotropy driven instabilities, and loss cone instabilities (by subtraction of two Maxwellians for a particular species) as well as a host of undamped/weakly damped modes. The Maxwellian assumption allows the dielectric tensor to be computed exactly based on summations over the Bessel functions and plasma dispersion function of Doppler shifted argument. As such, the physics of wave-particle resonance and Larmor radius are fully included in the model. The model is not specific to any plasma parameter regime or region of the magnetosphere.

[56] The model also allows generally for multiple species including populations of the same species with hot and cold temperatures. There is no requirement on these species other than that the sum of the ion densities should be the same as the electron density. In particular, a cold population is not required for application of the model.

[57] Although the presence of both cold and hot ion populations is commonly invoked for the generation of ion cyclotron waves in Earth's magnetosphere (and as noted the WHAMP code explicitly allows for this possibility), several studies have shown the existence of EMIC waves in Earth's magnetosheath that were driven only by hot plasma [*Anderson et al.*, 1991; *Anderson and Fuselier*, 1993, 1994;

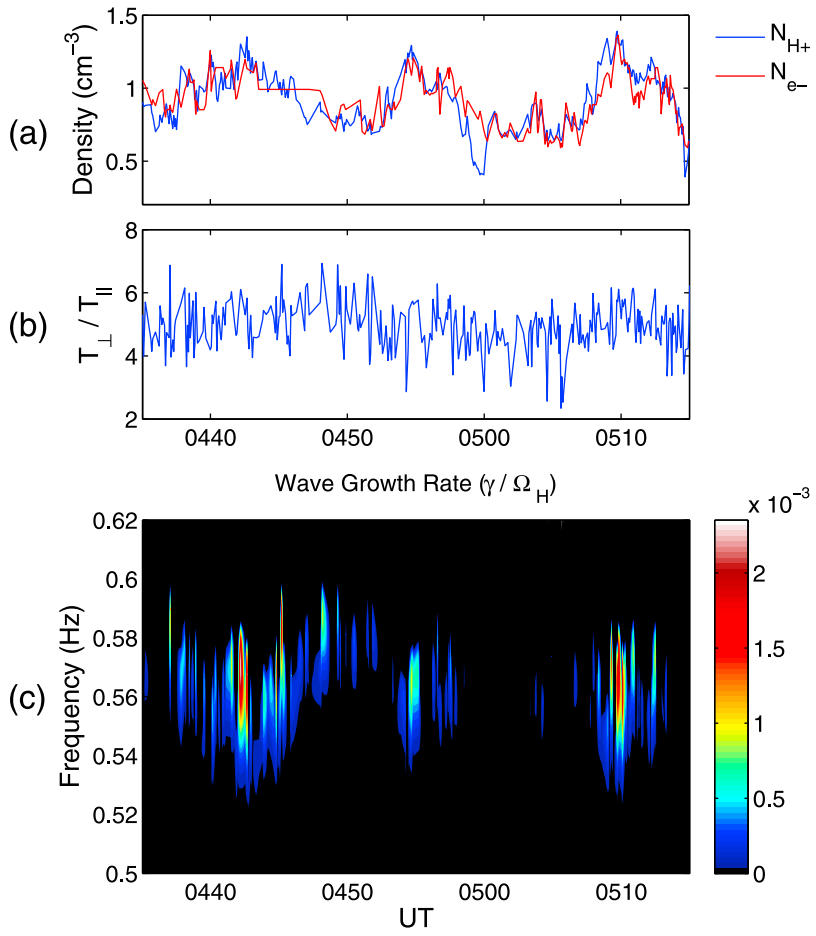

Figure 21. (a) Proton (N_{H+}) and electron (N_{e-}) densities; (b) proton temperature anisotropy; and (c) wave growth rate as a function of frequency and time from 0435 to 0515 UT 25 November 2002 at Cluster-4.

Denton et al., 1994; *Gary et al.*, 1994], and no cold population was observed during the wave events shown here despite the substantial antisunward convection of ~50 to over 100 km/s at times. As shown in Figure 10g, the velocity of the observed ion population streaming in the X_{GSM} direction (V_x) during the first wave event ranged from ~−70 to beyond −100 km/s, and the velocity in the Y_{GSM} direction was roughly half as large. The corresponding streaming velocity in the X_{GSM} direction during the second event (Figure 13g) was near −50 km/s, with again a value roughly half as large along Y_{GSM}. This means that the bulk of any cold population cannot be hidden; it should be seen at energies from a few eV to a few tens of eV. Because the HIA instrument measures down to 5 eV, the HIA data shown in Figures 10b and 13b shows no evidence of the existence of a separate cold ion population in association with the observed waves. Additional evidence for the absence of a hidden cold ion population comes from a comparison of ion density from HIA with electron density determined from WHISPER; the electron density was almost the same as the ion densities during each of these wave events (e.g., as shown for the second event in Figure 21a).

[58] We thus adopt the following assumptions: First, because both H^+ and O^+ bulk velocities are almost the same in Figure 13, we assume no relative electric drifts between the particle species. Second, particle densities and temperatures detected by Cluster 4 are used. However, the O^+ temperature (T_{O+}) fluctuates in time as shown in Figure 13, so we assume an average value of $T_{O+} \sim 30$ eV.

[59] Because of the absence of WHISPER data at Cluster 1, we only perform the wave instability analysis for Cluster 4. Although waves were observed at Cluster 4 from 0340 to 0520 UT (Figure 14), Cluster 4 temperature data were mostly unavailable between 0340 and 0435 UT. We thus show data and modeled growth rates from 0435 to 0515 UT only. Figure 21 shows the proton and electron densities (N_{H+} and N_{e-}) observed by Cluster 4 CIS and WHISPER (Figure 21a), proton temperature anisotropy ($T_\perp/T_{||}$) observed by CIS (Figure 21b), and calculated wave growth rates (γ/Ω_H) for $k_\perp = 0$ (Figure 21c). Because the observed wave propagation angles θ are $0 \le \theta < 45°$ in Figure 14e, we calculated the wave growth rates for different wave frequencies and propagation angles. Because the largest wave growth rate occurred for $k_\perp = 0$, and even for the relatively large angle of $\theta \sim 30°$ the wave growth rate was reduced only 20% from the maximum value (not shown), we only show the results for $k_\perp = 0$ here.

[60] We also used the oxygen ion density (N_{O+}) in the growth rate calculations; however, the observed N_{O+} was below 0.04 cm^{-3} throughout the interval, and we thus do not

plot N_{O+} in this figure. Because the time interval of N_{e-} is larger than N_{H+}, we linearly interpolated N_{e-} for the calculations. The N_{H+} and N_e traces show three density enhancements near 0442, 0455, and 0510 UT. During the density enhancement intervals, the temperature anisotropy (Figure 21b) remained at values between 4 and 6.

[61] Three intervals of enhanced wave growth rates are evident in Figure 21c, near 0437–0450, 0454–0458, and 0508–0513 UT. These fit well with the wave observations near 0442–0448, 0454–0500, and 0508–514 UT shown in Figure 14). For instance, both observations and calculated wave growth rates have strong peaks near 0441–0443, 0448, 0455–0456, and 0510–0512 UT. Because the temperature anisotropy during the wave events does not show large variations, these growth rate enhancements can be attributed to the high N_{H+} density. In these time intervals, the wave growth spatial scale ($L = (V_g - V_b)/\gamma$, where V_g is the wave group velocity, V_b is the beam velocity (assumed to be 100 km/s), and γ is the wave growth rate) is less than 0.1 R_E. As a result, EMIC waves can grow appreciably before they detune from the resonance condition required for wave growth as they propagate into regions of larger magnetic field. The three wave intervals shown in Figure 14 between 0435 and 0515 UT have a spatial extent at least 0.2 R_E, which is larger than the calculated wave growth spatial scale length, so they can grow appreciably within the observed unstable region. Although the calculated frequency range for instability (f = 0.53–0.6 Hz, $\Delta f \sim 0.07$) is narrower than the observations (f = 0.4–0.6 Hz, $\Delta f \sim 0.2$), it is expected that nonlocal effects will lead to the broadened spectrum because lower frequency waves can be generated in a region of lower magnetic field (tailward of the spacecraft's location) and propagate toward Earth.

[62] We also considered the O^+ temperature and anisotropy effects on wave generation in this event (not shown). However, because the O^+ density is relatively low compared to the total proton density, O^+ does not significantly affect the wave instability in this frequency range. Therefore, these results provide clear evidence that the waves are generated by the temperature anisotropy of the enhanced H^+ population.

6.3. Wave Mode

[63] The association of the observed left-hand polarized transverse (Alfvén mode) waves with streaming H^+ and O^+ ions suggests they might be generated by a left-hand beam resonant or ion cyclotron instability (propagating with or against the beam, respectively), as described by *Gary et al.* [1984]. Analysis of Poynting vector data showed the waves during the 30 September 2003 and 25 November 2002 events (Figures 3 and 14, respectively) were propagating earthward, antiparallel to **B**, that is, opposite to the direction of the ion streaming. This propagation direction, as well as the large temperature anisotropy shown in Figures 10, 13, and 20, supports the identification of these waves as EMIC waves. Unfortunately, a similar analysis could not be performed using the 3 November 2002 data because of large uncertainties in the electric field, due to the low number of available probes during this event.

[64] These waves are thus most probably the same type of waves as the "mantle waves" observed at lower altitudes, as reported earlier by *Dyrud et al.* [1997] and *Engebretson et al.* [2005]. In those studies as well, waves were observed during times of negative IMF Bz and/or large IMF By.

7. Summary and Conclusions

[65] Left-hand polarized, band-limited Alfvén mode Pc 1–2 waves have been observed during many passes of the Cluster spacecraft through the high-altitude lobe/mantle regions, near the magnetopause. In every case they were observed in association with tailward-streaming H^+ and O^+ ions with nearly identical bulk velocity. Both their asymmetric spatial occurrence and their IMF dependence (associated with large IMF By and/or negative IMF Bz) is consistent with a reconnection source for the protons, as was discussed recently in a study of streaming O^+ ions by *Liao et al.* [2010].

[66] Analysis of selected events shows that the waves are associated with large H^+ temperature anisotropies, and that the waves propagate opposite to the direction of the streaming ions. Both of these characteristics suggest that the ion cyclotron instability is the source of the observed waves. Similar streaming ion distributions are observed nearer to the tail midplane (lower Z and more negative X), but without wave activity. Consistent with this latter observation, modeling of the ion cyclotron instability using the WHAMP code showed that wave growth is larger for higher hot proton densities (higher plasma beta), as long as the proton temperature anisotropy does not change significantly.

[67] We have also observed intervals of intense broadband wave activity, as well as occasional intervals of intense, narrowband waves superposed on the broadband waves (e.g., 0030 to 0105 and 0215 to 0315 UT on 25 November 2002), in association with greatly increased ion densities. During these events H^+ and O^+ ions exhibit quite different velocities, probably consistent with their differing origins (H^+ ions from the solar wind via reconnection, O^+ ions from the ionosphere), and the anisotropies of the H^+ ions are lower than during narrowband wave events. We have presented evidence that these intervals occur outside the magnetopause, in the adjacent exterior cusp, boundary layer, or magnetosheath. Investigating the origin of these broadband noise events is, however, beyond the scope of this study.

[68] Although the existence of EMIC waves in this region of Earth's magnetosphere was not anticipated before they were first observed by *Dyrud et al.* [1997], we have shown that their generation, via the ion cyclotron instability, is basically consistent with known physics. The temperature anisotropy of ions in the plasma mantle was in fact noted in the first study of its characteristics [*Rosenbauer et al.*, 1975]. The physical consequences of the existence of these waves for other processes in the magnetotail, however, have not yet been explored.

[69] The unidirectional nature of these waves, and their source in ions streaming away from Earth, are quite different from the typical characteristics and location of Pc 1–2 waves, which propagate in both directions away from the near-equatorial closed-field-line regions of Earth's magnetosphere. Theoretical models of Pc 1–2 wave growth in these regions have typically assumed a modest, convective growth that can build up waves from multiple passes through the

unstable equatorial region, despite the more recently acknowledged lack of observational evidence for such multiple passes [e.g., as reviewed by *Guglielmi et al.*, 2001; *Fraser et al.*, 2006]. In the case of the mantle waves studied here, which are all observed to propagate Earthward, waves have only one pass through an extended region of instability. The existence of these waves thus underscores the need for further attention to absolute growth scenarios, both in the plasma mantle and in the equatorial middle and inner magnetosphere.

[70] As Figure 15f shows, however, the restrictions of Cluster's orbit did not permit observations of plasma mantle regions tailward of $X_{GSE} \sim -10\ R_E$. As a result, although our instability calculations indicate that Cluster did sample regions where wave growth is significant (although modest), we have no information about the tailward extent of the region of wave growth. In addition, although our observations have consistently shown Earthward wave propagation, we have no information about the direction(s) of propagation of waves generated considerably farther down the tail.

[71] Finally, in some but not all of the mantle wave events we have examined, the individual Cluster spacecraft saw similar but not identical waves and particle signatures. Simultaneous ground observations also showed local variations in frequency. Such multistation observations suggest that the regions of wave growth may be highly localized and variable. This spatial variability may reflect a similar spatial variability in the reconnection-related source of the protons that drive the waves, but investigation of this is again beyond the scope of this study.

[72] **Acknowledgments.** Work at Augsburg College was supported by NSF grants ATM-0827903, ANT-0838917, and ANT-0840133, and by the Minnesota Space Grant program. Work at the University of New Hampshire was supported by NSF grants ANT-0839938 and ANT-0838910. Operations at AGO P1 were supported by NSF grant ANT-0840158 to Siena College. The work of MJE on Cluster was initiated by a grant from the German Fulbright Commission. Work at the University of California, Berkeley was supported by NASA grant NNX08AF29G. Work at the University of Minnesota was supported by NASA grants NNX08AF28G and NAS5-01072. Work at the Institute of Atmospheric Physics was supported by GACR grant P209/11/P848. The work at Princeton University was supported by NASA grants (NNH09AM53I, NNH09AK63I, and NNH11AQ46I), NSF grant ATM0902730, and DOE contract DE-AC02-09CH11466. Work at the Technical University of Braunschweig was supported by the German Bundesministerium für Wirtschaft und Technologie and the Deutsche Zentrum für Luft- und Raumfahrt. Cluster work at IRAP was funded by CNES grants. The FGM and WHISPER data were accessed via the Cluster Active Archive. We thank the referees for many helpful comments and suggestions.

[73] Masaki Fujimoto thanks the reviewers for their assistance in evaluating this paper.

References

Anderson, B. J., and S. A. Fuselier (1993), Magnetic pulsations from 0.1 to 4.0 Hz and associated plasma properties in the Earth's subsolar magnetosheath and plasma depletion layer *J. Geophys. Res.*, *98*(A2), 1461–1479, doi:10.1029/92JA02197.

Anderson, B. J., and S. A. Fuselier (1994), Correction to "Magnetic pulsations from 0.1 to 4.0 Hz and associated plasma properties in the Earth's subsolar magnetosheath and plasma depletion layer," *J. Geophys. Res.*, *99*(A4), 6149–6150, doi:10.1029/93JA03041.

Anderson, B. J., and D. C. Hamilton (1993), Electromagnetic ion cyclotron waves stimulated by modest magnetospheric compressions, *J. Geophys. Res.*, *98*(A7), 11,369–11,382, doi:10.1029/93JA00605.

Anderson, B. J., S. A. Fuselier, and D. Murr (1991), Electromagnetic ion cyclotron waves observed in the plasma depletion layer, *Geophys. Res. Lett.*, *18*(11), 1955–1958, doi:10.1029/91GL02238.

Anderson, B. J., R. E. Erlandson, and L. J. Zanetti (1992a), A statistical study of Pc 1–2 magnetic pulsations in the equatorial magnetosphere, 1, equatorial occurrence distributions, *J. Geophys. Res.*, *97*(A3), 3075–3088, doi:10.1029/91JA02706.

Anderson, B. J., R. E. Erlandson, and L. J. Zanetti (1992b), A statistical study of Pc 1–2 magnetic pulsations in the equatorial magnetosphere, 2, wave properties, *J. Geophys. Res.*, *97*(A3), 3089–3101, doi:10.1029/91JA02697.

Balogh, A., et al. (2001), The Cluster magnetic field investigation: Overview of in-flight performance and initial results, *Ann. Geophys.*, *19*, 1207–1217.

Borovsky, J. E., M. F. Thomsen, and R. C. Elphic (1998), The driving of the plasma sheet by the solar wind, *J. Geophys. Res.*, *103*(A8), 17,617–17,639, doi:10.1029/97JA02986.

Broughton, M. C., M. J. Engebretson, K. H. Glassmeier, Y. Narita, A. Keiling, K.-H. Fornaçon, G. K. Parks, and H. Rème (2008), Ultra-low frequency waves and associated wave vectors observed in the plasma sheet boundary layer by Cluster, *J. Geophys. Res.*, *113*, A12217, doi:10.1029/2008JA013366.

Candidi, M., S. Orsini, and V. Formisano (1982), The properties of ionospheric O^+ ions as observed in the magnetotail boundary layer and northern plasma lobe, *J. Geophys. Res.*, *87*(A11), 9097–9106, doi:10.1029/JA087iA11p09097.

Candidi, M., S. Orsini, and J. L. Horwitz (1988), The tail lobe ion spectrometer: Theory and observations, *J. Geophys. Res.*, *93*(A12), 14,401–14,409, doi:10.1029/JA093iA12p14401.

Cargill, P. J., et al. (2005), Cluster at the magnetospheric cusps, *Space Sci. Rev.*, *118*, 321–366, doi:10.1007/s11214-005-3835-0.

Cladis, J. B. (1986), Parallel acceleration and transport of ions from polar ionosphere to plasma sheet, *Geophys. Res. Lett.*, *13*(9), 893–896, doi:10.1029/GL013i009p00893.

Cladis, J. B., H. L. Collin, O. W. Lennartsson, T. E. Moore, W. K. Peterson, and C. T. Russell (2000), Observations of centrifugal acceleration during compression of magnetosphere, *Geophys. Res. Lett.*, *27*(7), 915–918, doi:10.1029/1999GL010737.

Décréau, P. M. E., et al. (1997), WHISPER, a resonance sounder and wave analyser: Performances and perspectives for the CLUSTER mission, *Space Sci. Rev.*, *79*, 157–193, doi:10.1023/A:1004931326404.

Denton, R. E., S. P. Gary, B. J. Anderson, S. A. Fuselier, and M. K. Hudson (1994), Low-frequency magnetic fluctuation spectra in the magnetosheath and plasma depletion layer, *J. Geophys. Res.*, *99*(A4), 5893–5901, doi:10.1029/93JA02729.

Denton, R. E., M. J. Engebretson, A. Keiling, A. P. Walsh, S. P. Gary, P. M. E. Décréau, C. A. Cattell, and H. Rème (2010), Multiple harmonic ULF waves in the plasma sheet boundary layer: Instability analysis, *J. Geophys. Res.*, *115*, A12224, doi:10.1029/2010JA015928.

Dyrud, L. P., M. J. Engebretson, J. L. Posch, W. J. Hughes, H. Fukunishi, R. L. Arnoldy, P. T. Newell, and R. B. Horne (1997), Ground observations and possible source regions of two types of Pc 1–2 micropulsations at very high latitudes, *J. Geophys. Res.*, *102*(A12), 27,011–27,027, doi:10.1029/97JA02191.

Engebretson, M. J., N. Lin, W. Baumjohann, H. Lühr, B. J. Anderson, L. J. Zanetti, T. A. Potemra, R. L. McPherron, and M. G. Kivelson (1991), A comparison of ULF fluctuations in the solar wind, magnetosheath, and dayside magnetosphere, 1. Magnetosheath morphology, *J. Geophys. Res.*, *96*(A3), 3441–3454, doi:10.1029/90JA02101.

Engebretson, M. J. et al. (1997), The United States automatic geophysical observatory (AGO) program in Antarctica, in *Satellite-Ground Based Coordination Sourcebook*, *ESA-SP-1198*, edited by M. Lockwood et al., pp. 65–99, ESTEC, Noordwijk, Netherlands.

Engebretson, M. J., T. G. Onsager, D. E. Rowland, R. E. Denton, J. L. Posch, C. T. Russell, P. J. Chi, R. L. Arnoldy, B. J. Anderson, and H. Fukunishi (2005), On the sources of Pc 1–2 waves in the plasma mantle, *J. Geophys. Res.*, *110*, A06201, doi:10.1029/2004JA010515.

Engebretson, M. J., J. Moen, J. L. Posch, F. Lu, M. R. Lessard, H. Kim, and D. A. Lorentzen (2009), Searching for ULF signatures of the cusp: Observations from search coil magnetometers and auroral imagers in Svalbard, *J. Geophys. Res.*, *114*, A06217, doi:10.1029/2009JA014278.

Engebretson, M. J., C. R. G. Kahlstorf, J. L. Posch, A. Keiling, A. P. Walsh, R. E. Denton, M. C. Broughton, C. J. Owen, J.-H. Fornaçon, and H. Rème (2010), Multiple harmonic ULF waves in the plasma sheet boundary layer observed by Cluster, *J. Geophys. Res.*, *115*, A12225, doi:10.1029/2010JA015929.

Escoubet, C. P., M. Fehringer, and M. Goldstein (2001), The Cluster mission, *Ann. Geophys.*, *19*, 1197–1200.

Fraser, B. J., T. M. Loto'aniu, and H. J. Singer (2006), Electromagnetic ion cyclotron waves in the magnetosphere, in *Magnetospheric ULF Waves: Synthesis and New Directions*, *Geophys. Monogr. Ser.*, vol. 169, edited by K. Takahashi et al., pp. 195–212, AGU, Washington, D.C., doi:10.1029/169GM13.

Fuselier, S. A., B. J. Anderson, S. P. Gary, and R. E. Denton (1994), Inverse correlations between the ion temperature anisotropy and plasma beta in the Earth's quasi-parallel magnetosheath, *J. Geophys. Res.*, *99*(A8), 14,931–14,936, doi:10.1029/94JA00865.

Gary, S. P., C. W. Smith, M. A. Lee, M. L. Goldstein, and D. W. Forslund (1984), Electromagnetic ion beam instabilities, *Phys. Fluids*, *27*, 1852–1863, doi:10.1063/1.864797.

Gary, S. P., B. J. Anderson, R. E. Denton, S. A. Fuselier, and M. E. McKean (1994), A limited closure relation for anisotropic plasmas from the Earths magnetosheath, *Phys. Plasmas*, *1*(5), 1676–1684, doi:10.1063/1.870670.

Gary, S. P., M. F. Thomsen, L. Yin, and D. Winske (1995), Electromagnetic proton cyclotron instability: Interactions with magnetospheric protons, *J. Geophys. Res.*, *100*(A11), 21,961–21,972, doi:10.1029/95JA01403.

Gosling, J., D. Baker, S. Bame, W. Feldman, R. Zwickl, and E. Smith (1985), North-south and dawn-dusk plasma asymmetries in the distant tail lobes: ISEE 3, *J. Geophys. Res.*, *90*(A7), 6354–6360, doi:10.1029/JA090iA07p06354.

Guglielmi, A., J. Kangas, and A. Potapov (2001), Quasiperiodic modulation of the Pc1 geomagnetic pulsations: An unsettled problem, *J. Geophys. Res.*, *106*(A11), 25,847–25,855, doi:10.1029/2001JA000136.

Gustafsson, G., et al. (2001), First results of electric field and density observations by Cluster EFW based on initial months of operation, *Ann. Geophys.*, *19*, 1219–1240, doi:10.5194/angeo-19-1219-2001.

Hardy, D. A., H. K. Hills, and J. W. Freeman (1975), A new plasma regime in the distant geomagnetic tail, *Geophys. Res. Lett.*, *2*(5), 169–172, doi:10.1029/GL002i005p00169.

Hirahara, M., T. Mukai, T. Terasawa, S. Machida, Y. Saito, T. Yamamoto, and S. Kokubun (1996), Cold dense ion flows with multiple components observed in the distant tail lobe by Geotail, *J. Geophys. Res.*, *101*(A4), 7769–7784, doi:10.1029/95JA03165.

Horwitz, J. L. (1986), The tail lobe ion spectrometer, *J. Geophys. Res.*, *91*(A5), 5689–5699, doi:10.1029/JA091iA05p05689.

Horwitz, J., and M. Lockwood (1985), The cleft ion fountain: A two-dimensional kinetic model, *J. Geophys. Res.*, *90*(A10), 9749–9762, doi:10.1029/JA090iA10p09749.

Kangas, J., A. Guglielmi, and O. Pokhotelov (1998), Morphology and physics of short-period magnetic pulsations—A review, *Space Sci. Rev.*, *83*, 435–512, doi:10.1023/A:1005063911643.

Knipp, D., S. Eriksson, L. Kilcommons, G. Crowley, J. Lei, M. Hairston, and K. Drake (2011), Extreme Poynting flux in the dayside thermosphere: Examples and statistics, *Geophys. Res. Lett.*, *38*, L16102, doi:10.1029/2011GL048302.

Lavraud, B., et al. (2002), Cluster observations of the exterior cusp and its surrounding boundaries under northward IMF, *Geophys. Res. Lett.*, *29*(20), 1995, doi:10.1029/2002GL015464.

Lavraud, B., et al. (2004), Cluster survey of the high-altitude cusp properties: A three-year statistical study, *Ann. Geophys.*, *22*(8), 3009–3019, doi:10.5194/angeo-22-3009-2004.

Lavraud, B., et al. (2005), High-altitude cusp flow dependence on IMF orientation: A 3-year Cluster statistical study, *J. Geophys. Res.*, *110*, A02209, doi:10.1029/2004JA010804.

Li, W., D. Knipp, J. Lei, and J. Raeder (2011), The relation between dayside local Poynting flux enhancement and cusp reconnection, *J. Geophys. Res.*, *116*, A08301, doi:10.1029/2011JA016566.

Liao, J., L. M. Kistler, C. Mouikis, B. Klecker, I. Dandouras, and J.-C. Zhang (2010), Statistical study of O^+ transport from the cusp to the lobes with Cluster CODIF data, *J. Geophys. Res.*, *115*, A00J15, doi:10.1029/2010JA015613.

Lui, A. T. Y. (1987), Road map to magnetotail domains, in *Magnetotail Physics*, edited by A. T. Y. Lui, pp. 3–9, Johns Hopkins Univ. Press, Baltimore, Md.

Menk, F. W., B. J. Fraser, H. J. Hansen, P. T. Newell, C.-I. Meng, and R. J. Morris (1992), Identification of the magnetospheric cusp and cleft using Pc 1–2 pulsations, *J. Atmos. Terr. Phys.*, *54*, 1021–1042, doi:10.1016/0021-9169(92)90069-W.

Orsini, S., M. Candidi, and H. Balsiger (1987), Composition and velocity of ions streaming in the plasma mantle and in the lobe, in *Magnetotail Physics*, edited by A. T. Y. Lui, pp. 239–243, Johns Hopkins Univ. Press, Baltimore, Md.

Pilipp, W. G., and G. Morfill (1978), The formation of the plasma sheet resulting from plasma mantle dynamics, *J. Geophys. Res.*, *83*(A12), 5670–5678, doi:10.1029/JA083iA12p05670.

Rème, H., et al. (2001), First multispacecraft ion measurements in and near the Earth's magnetosphere with the identical Cluster ion spectrometry (CIS) experiment, *Ann. Geophys.*, *19*, 1303–1354.

Rönnmark, K. (1982), Waves in homogeneous, anisotropic multicomponent plasmas (WHAMP), *Kiruna Geophys. Inst. Rep. 179*, Kiruna Geophys. Inst., Kiruna, Sweden.

Rönnmark, K. (1984), Ray tracing in dissipative media, *Ann. Geophys.*, *2*, 57–60.

Rosenbauer, H., H. Grünwaldt, M. D. Montgomery, G. Paschmann, and N. Sckopke (1975), Heos 2 plasma observations in the distant polar magnetosphere: The plasma mantle, *J. Geophys. Res.*, *80*(19), 2723–2737, doi:10.1029/JA080i019p02723.

Santolík, O., F. Lefeuvre, M. Parrot, and J. L. Rauch (2001), Complete wave-vector directions of electromagnetic emissions: Application to INTERBALL-2 measurements in the nightside auroral zone, *J. Geophys. Res.*, *106*(A7), 13,191–13,201, doi:10.1029/2000JA000275.

Santolík, O., M. Parrot, and F. Lefeuvre (2003), Singular value decomposition methods for wave propagation analysis, *Radio Sci.*, *38*(1), 1010, doi:10.1029/2000RS002523.

Seki, K., M. Hirahara, T. Terasawa, I. Shinohara, T. Mukai, Y. Saito, S. Machida, T. Yamamoto, and S. Kokubun (1996), Coexistence of Earth-origin O+ and solar wind-origin H^+/He^{++} in the distant magnetotail, *Geophys. Res. Lett.*, *23*(9), 985–988, doi:10.1029/96GL00768.

Seki, K., T. Terasawa, M. Hirahara, and T. Mukai (1998), Quantification of tailward cold O^+ beams in the lobe/mantle regions with Geotail data: Constraints on polar O^+ outflows, *J. Geophys. Res.*, *103*(A12), 29,371–29,381, doi:10.1029/98JA02463.

Seki, K., M. Hirahara, T. Terasawa, T. Mukai, and S. Kokubun (2000), Origin and dynamics of multi-component (H^+/He^{++}/O^+) ion flows in the lobe/mantle regions, *Adv. Space Res.*, *25*, 1581–1590, doi:10.1016/S0273-1177(99)00671-7.